ELECTROMAGNETIC ION/ION INSTABILITIES AND THEIR CONSEQUENCES IN SPACE PLASMAS: A REVIEW

S. PETER GARY

Los Alamos National Laboratory, Los Alamos, NM 87545, U.S.A.

(Received 26 April, 1989; revised 27 July, 1989)

Abstract. This paper reviews recent research on the theory and computer simulations of electromagnetic ion/ion instabilities and their consequences in space plasmas. 'Ion/ion' instabilities are growing modes in a collisionless plasma driven unstable by the relative streaming velocity $\mathbf{v}_0$ of two distinct ion components such that $\mathbf{v}_0$ is parallel or antiparallel to the uniform background magnetic field $\mathbf{B}_0$. The space physics regimes which display enhanced fluctuations due to these instabilities and which are reviewed in this paper include the solar wind, the terrestrial foreshock, the plasma sheet boundary layer, and distant cometary environments.

1. Introduction

Whenever two plasmas stream through one another parallel to an average magnetic field, the non-Maxwellian character of the distribution functions can lead to plasma instabilities, enhanced field fluctuations, and wave-particle scattering. Electron/electron instabilities typically correspond to high frequencies, fast growth rates and rapid electron scattering to relative isotropization. Electron/ion instabilities characteristically grow at lower frequencies, have smaller growth rates, and correspond to wave-particle scattering which typically tends to pull electrons to the ion center of mass frame on somewhat longer time-scales. Electrostatic ion/ion instabilities can compete in growth frequencies and growth rates with electrostatic electron/ion modes, but they require conditions such as $T_i \ll T_e$ which are not often available under many space plasma conditions and, hence, are often not effective in scattering ions. Although electromagnetic ion/ion instabilities typically have the lowest frequencies and growth rates (of the order or less than the ion cyclotron frequency), they are more robust (i.e., less sensitive to plasma parameters) than their electrostatic counterparts, can grow to the largest fluctuating field energy densities of any of the plasma streaming modes, and, given sufficient growth length or time, can strongly scatter ion components to isotropy and eventually to thermalization.

The near-Earth space environment not only often provides the counterstreaming plasma conditions necessary to excite electromagnetic ion/ion instabilities but also the large spatial extent which their ponderous growth requires to reach efficacy. Thus these modes are observed in, and contribute to the plasma dynamics of, many different space plasma regions, including the high speed solar wind, the foreshocks of planetary bow and interplanetary shocks, the plasma sheet boundary layer of the terrestrial magnetotail, and the distant environment of comets. The widespread occurrence of these modes has stimulated substantial theoretical and simulation research of their properties;

Space Science Reviews **56:** 373–415, 1991.

it is the purpose of this paper to review this research and to place it in an appropriate observational context.

We here establish definitions and notations which, unless stated otherwise, will be used throughout this paper. With respect to the observations, we emphasize fluctuations near and below the proton and other ion cyclotron frequencies, which domain we term 'low frequency', and thermal and suprathermal ion distributions up to a few tens of keV which are most likely to interact with such fluctuations. With respect to our theoretical models, unless stated otherwise we consider a homogeneous, charge neutral plasma with a uniform magnetic field $\mathbf{B}_0 = \hat{\mathbf{z}} B_0$ with $B_0 > 0$ and no ambient electric field. The following symbols are defined for the jth component: the plasma frequency, $\omega_j \equiv (4\pi n_j e_j^2/m_j)^{1/2}$; the cyclotron frequency, $\Omega_j \equiv e_j B/m_j c$; the Debye wave number, $k_j \equiv (4\pi n_j e_j^2/T_j)^{1/2}$; the thermal speed $v_j \equiv (T_j/m_j)^{1/2}$; the (signed) thermal gyroradius $a_j \equiv v_j/\Omega_j$; and beta $\beta_j \equiv 8\pi n_0 T_j/B_0^2$ where n_0 is the total electron or ion density. The Boltzmann factor k_B is understood to multiply the temperatures T_j throughout this paper.

We usually consider a two species plasma, denoting the electrons by 'e' and the quantities which refer to ions in general as subscripted with 'i'. The ions usually consist of two components: a more dense core (subscript 'c') and the more tenuous beam (subscript 'b'). We denote the special case of a cometary ion shell distribution by the subscript 's', and the subscript 'p' denotes protons. The square of the Alfvén speed is $v_A^2 = B_0^2/4\pi n_0 m_p$. The subscripts '$\parallel$' and '$\perp$' denote parallel and perpendicular to $\mathbf{B}_0$, respectively; temperatures without such subscripts are understood to be $T_{\parallel j}$. We use $\mathbf{v}_{0j} = \hat{\mathbf{z}} v_{0j}$ to represent the drift velocity of the jth component along $\mathbf{B}_0$. We take the zeroth-order plasma to be charge neutral, $n_e = n_i$, we consider only the case of zero current, $\Sigma_j e_j n_j \mathbf{v}_{0j} = 0$, and we work in the zero-momentum frame $\Sigma_j n_j \mathbf{v}_{0j} = 0$, so that, if $m_b = m_c$, $\mathbf{v}_{0e} = 0$. We denote the beam-core relative drift as $\mathbf{v}_0 \equiv \mathbf{v}_{0b} - \mathbf{v}_{0c}$.

The rest of this paper is structured as follows: Section 2 outlines the observational space plasma evidence which has led to the theoretical study of electromagnetic ion/ion instabilities. Section 3 further defines the notation and the model used for the linear theory of this paper. Section 4 uses results of computer solutions of the linear electromagnetic dispersion equation to review the current state of linear theory of low-frequency electromagnetic ion/ion instabilities in a homogeneous Vlasov plasma. Section 5 reviews published quasilinear theories and Section 6 is a review of the published literature concerning computer simulations of such instabilities and their consequences. Finally, Section 7 discusses the applications of both theory and simulations to several different space plasma regimes.

2. Some Experimental Results

Evidence for the existence of electromagnetic ion/ion instabilities in space plasmas consists of observations of both suprathermal ion distribution functions and enhanced low-frequency magnetic fluctuations. In this section we briefly summarize both types of observations, as preparation for the relevant theory and simulation results to be discussed later in this review.

2.1. SOLAR WIND

Studies of ion distributions in the solar wind near 1 AU have shown the frequent existence of two component proton distributions during and immediately after most high-speed streams (Feldman *et al.*, 1973, 1974). Observations from interplanetary probes have yielded similar results (Goodrich and Lazarus, 1976); in particular, Helios solar probe measurements have demonstrated that two distinct proton components exist in the high speed solar wind between 0.3 and 1.0 AU (Marsch *et al.*, 1982). The two peaks generally correspond to components of unequal densities (typically, at 1 AU $n_b \simeq 0.25 n_c$). The less dense beam component moves along the interplanetary magnetic field $\mathbf{B}_0$ in a direction generally away from the Sun, and a drift speed relative to the solar wind ions which typically satisfies $v_0 \sim v_A$. The two peaks are often clearly resolvable; furthermore, the solar wind or core component typically exhibits $T_{\parallel c} < T_{\perp c}$ in high-speed streams (Bame *et al.*, 1975; Marsch *et al.*, 1982).

We are not aware of any observations demonstrating enhanced magnetic fluctuation levels in association with such distributions. However, the observations of Neugebauer (1975) and Unti and Russell (1976) indicate small but statistically significant enhancements of solar wind ion density and flux fluctuations at $ka_p \simeq 1$, and Tsurutani *et al.* (1987b) report the occasional presence of weak ($|\delta\mathbf{B}| \ll |\mathbf{B}_0|$) or moderate ($|\delta\mathbf{B}| < |\mathbf{B}_0|$) amplitude magnetic fluctuations near the proton cyclotron frequency in association with high speed streams.

2.2. THE TERRESTRIAL BOW SHOCK

A variety of suprathermal ion distributions are observed in the terrestrial foreshock, that portion of the upstream region which is accessible to energetic ions from the bow shock. Upstream of the quasi-perpendicular bow shock ($\theta_{Bn} > 45°$ where θ_{Bn} is the angle between the upstream $\mathbf{B}_0$ and the local shock normal $\hat{\mathbf{n}}$), field-aligned beams are observed which are tenuous ($n_b \simeq 0.01 n_c$) (Bonifazi and Moreno, 1981), anisotropic ($T_{\perp b} \gg T_{\parallel b}$) (Paschmann *et al.*, 1981), of high speed ($v_{0b} \gtrsim 10 v_A$), and relatively cool ($T_c < T_b < \frac{1}{2} m_p v_{0b}^2$); no associated low-frequency magnetic fluctuations are observed above the solar wind background. Somewhat downstream of the field-aligned beam observations, suprathermal ions are often described as 'intermediate': they are warmer than the field-aligned beams, have a characteristic beam- or crescent-shape in velocity space, and are associated with moderate ($|\delta\mathbf{B}| < |\mathbf{B}_0|$) amplitude low-frequency magnetic fluctuations which are relatively monochromatic and right-hand elliptically polarized in the solar wind frame (Hoppe and Russell, 1983). The observations suggest that the intermediate ions are field-aligned beams which have been scattered in both pitch-angle and energy (Paschmann *et al.*, 1981). Upstream of the quasi-parallel bow shock ($\theta_{Bn} \lesssim 45°$), energetic ions are still observed to be tenuous ($n_b \simeq 0.01 n_c$) (Bonifazi and Moreno, 1981), but are now typically 'diffuse' (Gosling *et al.*, 1978) with weak anisotropies ($T_{\perp b} \simeq T_{\parallel b}$), smaller drift speeds ($v_0 \sim v_A$) and much higher temperatures ($T_c < \frac{1}{2} m_p v_{0b}^2 \ll T_b$). The associated low-frequency magnetic fluctuations are typically observed to be strongly enhanced ($|\delta\mathbf{B}| \sim |\mathbf{B}_0|$) (Fairfield, 1969; Hoppe *et al.*, 1981),

are predominantly right-hand polarized in the solar wind rest frame (Le *et al.*, 1989a), and have the characteristic appearance of a steepened wave or 'shocklet' with a shorter wavelength wave packet on its leading edge (Hoppe *et al.*, 1981). A fourth category of suprathermal ions, termed 'gyrating ions' (Thomsen *et al.*, 1985), correspond to distributions with peaks which lie at nonzero pitch-angles relative to $\mathbf{B}_0$. Ions of this type that are found well away from the bow shock are typically non-gyrotropic and are usually associated with large amplitude, monochromatic low-frequency magnetic fluctuations (Fuselier *et al.*, 1986b). Thomsen (1985) has provided a comprehensive review of the subject of foreshock suprathermal ions.

Ion beams are also sometimes observed within the bow shock itself. By comparison with the field-aligned beams of the foreshock they are relatively cool ($T_b \simeq T_c$) and relatively dense ($n_b \sim n_c$). These beams are thought to be generated by specular reflection at the shock, and are observed at both quasi-perpendicular shocks (Paschmann *et al.*, 1982; Sckopke *et al.*, 1983) and quasi-parallel shocks (Gosling *et al.*, 1989b). Under quasi-parallel conditions, specularly reflected ions are more nearly magnetic-field aligned and can escape upstream (Gosling *et al.*, 1982) where they may give rise to ion/ion instabilities. However, because quasi-parallel shocks are usually observed with a diffuse ion component and the associated enhanced low-frequency fluctuations, no clear correlation between specularly reflected ions and enhanced fluctuations has yet been established.

2.3. Other shocks

Observations both upstream and downstream of interplanetary shocks indicate much less variety in the suprathermal ion distributions: they are typically observed to be very hot and diffuse-like (Gosling, 1983; Gosling *et al.*, 1984). These distributions appear in association with enhanced low-frequency magnetic fluctuations (Sanderson *et al.*, 1985), with predominantly right-hand polarization in the solar wind frame, more moderate amplitudes ($|\delta\mathbf{B}| < |\mathbf{B}_0|$), propagation more parallel to $\mathbf{B}_0$, and less compressibility than fluctuations observed in the terrestrial foreshock (Tsurutani *et al.*, 1983; Viñas *et al.*, 1984). Enhanced magnetic fluctuations also have been observed upstream of the bow shocks of several different planets including Mercury (Fairfield and Behannon, 1976), Venus (Hoppe and Russell, 1982), Jupiter (Smith *et al.*, 1976, 1983; Goldstein *et al.*, 1983; Bavassano-Cattaneo *et al.*, 1987), and Saturn (Behannon *et al.*, 1985).

2.4. The plasma sheet boundary layer

The plasma sheet boundary layer is the region of the Earth's magnetotail which lies between a lobe, a region of relatively low plasma density and high magnetic field intensity, and the central plasma sheet, the domain of hot, high density plasma and less intense magnetic fields. Ion distribution functions in near-Earth ($\lesssim 20R_E$) sections of this layer are observed to consist of an anisotropic, earthward streaming ion component or of two anisotropic counterstreaming ion components (DeCoster and Frank, 1979; Forbes *et al.*, 1981; Eastman *et al.*, 1984; Takahashi and Hones, 1988). Weak

($|\delta\mathbf{B}| \ll |\mathbf{B}_0|$) low-frequency magnetic fluctuation spectra in the near-Earth portion of this boundary layer have been described by Russell (1972); his observations suggest a decrease of fluctuation amplitude with distance down the tail.

In the plasma sheet boundary layer of the far magnetotail, the $200R_E$-distant passes of ISEE-3 did not yield any thermal or suprathermal ion distribution functions, but did show a correlation between moderately strong, low-frequency magnetic fluctuations ($|\delta\mathbf{B}| < |\mathbf{B}_0|$) (Tsurutani and Smith, 1984) and enhanced fluxes of highly anisotropic, energetic (> 35 keV) ions (Tsurutani *et al.*, 1985). The fluctuations are generally magnetic-field-aligned, right-hand circularly polarized waves, and satisfy $0.2 \lesssim \omega_r/\Omega_p \lesssim 1.5$.

2.5. Cometary environments

Observations in distant cometary environments, i.e., beyond the bow shock or bow wave, have demonstrated large-amplitude, low-frequency fluctuations in the magnetic field amplitude (Smith *et al.*, 1986; Riedler *et al.*, 1986; Saito *et al.*, 1986; Neubauer *et al.*, 1986; Yumoto *et al.*, 1986), the plasma density (Bame *et al.*, 1986; Gosling *et al.*, 1986), and the solar wind proton velocity (Johnstone *et al.*, 1987). These fluctuations grow from the relatively low ambient solar wind amplitudes at great distances to maximum amplitude in the vicinity of the bow wave or shock. If $\alpha \lesssim 60°$, where α is the angle between the solar wind velocity $\mathbf{v}_{sw}$ and the interplanetary magnemtic field $\mathbf{B}_0$, the spacecraft is usually in what Glassmeier *et al.* (1989) term the quasi-parallel region of the cometary environment. In this region, magnetic fluctuations are observed to be of largest amplitude near the water-group-ion gyrofrequency (Tsurutani and Smith, 1986a; Glassmeier *et al.*, 1989), and are predominantly linearly polarized close to the bow wave/shock (Tsurutani *et al.*, 1987a; Johnstone *et al.*, 1987). The magnetic fluctuations at Giacobini–Zinner are different from those observed at Halley in two important ways: their maximum amplitudes are large ($|\delta\mathbf{B}| \sim |\mathbf{B}_0|$), as contrasted with the more moderate amplitudes near Halley, and they show evidence of nonlinear steepening to form 'shocklets' and the associated short wavelength wave packets (Tsurutani and Smith, 1986b) which Le *et al.* (1989a) have shown are very similar to the shocklets and wave packets observed in the terrestrial foreshock.

Cometary ion observations at Comet Halley (Mukai *et al.*, 1986; Wilken *et al.*, 1987; Neugebauer *et al.*, 1987a) show shell-like velocity distributions that are relatively broad in pitch-angle. More recent, more detailed analyses show cometary ion distributions in the form of partial shells at large distances from the comet, which become scattered to complete shells either well upstream of the shock in the case of water group ions (Coates *et al.*, 1989), or just before the shock in the case of protons (Neugebauer *et al.*, 1989). For both cometary ion species, pitch-angle scattering to isotropy is observed to take place more rapidly than energy diffusion to thermalization.

Finally, we mention a peculiar but apparently widespread phenomenon: the observation of multiple and evenly spaced spectral peaks in the magnetic fluctuations in both the Jovian (Smith *et al.*, 1983) and terrestrial (Smith *et al.*, 1985) foreshocks, as well as in the distant cometary environment (Glassmeier *et al.*, 1989).

3. Linear Theory: The Model

In this section we establish the notation and definitions of quantities associated with field fluctuations, then state the different distribution functions and their associated conductivities used in this paper.

All fluctuating quantities are assumed to vary in time as $\exp(-i\omega t)$ where a complex frequency $\omega = \omega_r + i\gamma$ is assumed. The fluctuating fields are Fourier transformed in the $y - z$ plane so the wavevector is $\mathbf{k} = \hat{\mathbf{y}}k_y + \hat{\mathbf{z}}k_z$ and θ represents the angle between $\mathbf{k}$ and $\mathbf{B}_0$. We take $k_y \geq 0$ and $k_z \geq 0$; a reversal of the direction of propagation corresponds to a change in the sign of ω_r. Here $k = |\mathbf{k}|$.

For an arbitrary direction of $\mathbf{k}$, the electromagnetic dispersion equation in a homogeneous plasma is the solution of a 3×3 determinant, Equation (A.4) of the Appendix. For the less general but more tractible case of propagation parallel or antiparallel to the background magnetic field, i.e., $\mathbf{k} \times \mathbf{B}_0 = 0$, the linear dispersion equation is

$$\omega^2 - k^2c^2 + k^2c^2 \sum_j S_j^{\pm}(\mathbf{k}, \omega) = 0\,, \tag{1}$$

where the sum is over the different plasma components and the dimensionless conductivity of the jth component is

$$S_j^{\pm}(\mathbf{k}, \omega) = -\frac{\omega_j^2}{2k^2c^2n_j} \int \mathrm{d}^3v\, v_\perp \left(k_z v_\perp \frac{\partial f_j^{(0)}}{\partial v_z} + (\omega - k_z v_z) \frac{\partial f_j^{(0)}}{\partial v_\perp} \right) \times$$

$$\times (k_z v_z - \omega \mp \Omega_j)^{-1}\,. \tag{2}$$

The $\pm$ sign on $S_j^{\pm}$ corresponds to a choice of fluctuation helicity; the $+$ corresponds to positive helicity, whereas the $-$ represents negative helicity. If we consider $k_z > 0$ and $\omega_r > 0$, the plus sign also represents right-hand circular polarization, whereas the negative sign corresponds to left-hand circular polarization.

We follow the plasma physics definition of polarization, which defines right- or left-handed to be the sense of rotation in time of a fluctuating field vector when viewed from the plasma or center of mass frame of reference and in the direction parallel to the magnetic field. Under this definition, a right-hand mode propagating either parallel or anti-parallel to $\mathbf{B}_0$ possesses fluctuating field vectors that rotate in the same sense as the gyromotion of an electron, and corresponds to the magnetosonic/whistler wave in a stable plasma at $\mathbf{k} \times \mathbf{B}_0 = 0$. Similarly, a left-hand mode rotates in the same sense as a gyrating ion and corresponds to the Alfvén/ion cyclotron mode in a stable plasma at $k_y = 0$.

For $\mathbf{k} = \hat{\mathbf{y}}k_y + \hat{\mathbf{z}}k_z$, the generalization of the Stix (1962) polarization to arbitrary sign of the real frequency is

$$P = \frac{E_y^{(1)}}{iE_x^{(1)}} \frac{\omega_r}{|\omega_r|}\,. \tag{3}$$

In the particular case of $\mathbf{k} \times \mathbf{B}_0 = 0$, P is real:

$$P = \pm \frac{\omega_r}{|\omega_r|} . \tag{4}$$

Then $P = +1$ corresponds to a right-hand circularly polarized mode, and $P = -1$ to a left-hand circular mode. In the more general case of oblique propagation, polarization is elliptic and $\mathrm{Re}(P) > 0$ corresponds to right-hand, $\mathrm{Re}(P) < 0$ to left-hand waves.

As we demonstrate below, the advantage of using polarization as a wave identifier is that, at propagation which is not strongly oblique to $\mathbf{B}_0$, it is directly related to a particular mode with specific dispersion properties. In contrast, note that polarization is a frequency-dependent quantity and is therefore not invariant under a Galilean transformation. The reader is advised that the theoretical polarizations discussed throughout this paper are computed in the center of mass or plasma frame, and may not be directly comparable to the spacecraft frame polarizations measured in a flowing plasma such as the solar wind.

The helicity is an alternative quantity for describing the 'handedness' of a wave. In contrast to the polarization, however, it describes the sense of rotation with respect to $\mathbf{k}$ of the fluctuating fields in space at a fixed time. Furthermore, since it is a function of wave number, rather than frequency, it is not subject to a Doppler shift and is independent of the frame in which it is measured. However, as we shall demonstrate, the helicity has the disadvantage that it is not unique for a particular mode; e.g., the magnetosonic wave may have either positive or negative helicity, depending on the direction of propagation.

The helicity density is defined by (Matthaeus and Goldstein, 1982)

$$H_m \equiv \langle \mathbf{A} \cdot \mathbf{B} \rangle , \tag{5}$$

where $\mathbf{A}$ is the vector potential, $\mathbf{B} = \nabla \times \mathbf{A}$ and the angular brackets represent an ensemble average over waves of random phase. The results of this paper are reported in terms of the dimensionless helicity of the fluctuating fields

$$\sigma(\mathbf{k}) = \frac{k \langle \mathbf{A}^{(1)}(\mathbf{k}) \cdot \mathbf{B}^{(1)}(\mathbf{k}) \rangle}{|\mathbf{B}^{(1)}|^2} . \tag{6}$$

If one imposes the Coulomb gauge ($\nabla \cdot \mathbf{A} = 0$), it then follows from Equation (6) that, for the single Fourier component considered in this paper,

$$\sigma(\mathbf{k}) = \frac{2}{k |E_T^{(1)}|^2} \mathrm{Im}(k_y E_x^{(1)} E_z^{(1)*} - k_z E_x^{(1)} E_y^{(1)*}) , \tag{7}$$

where $\mathbf{E}_T^{(1)} \equiv \mathbf{E}^{(1)} - \hat{\mathbf{k}}(\hat{\mathbf{k}} \cdot \mathbf{E}^{(1)})$, the fluctuating electric field component transverse to $\mathbf{k}$, is obtained from Faraday's equation:

$$\frac{|\mathbf{E}_T^{(1)}|^2}{|\mathbf{B}^{(1)}|^2} = \frac{|\omega|^2}{k^2 c^2} . \tag{8}$$

In the limit of $\mathbf{k} \times \mathbf{B}_0 = 0$, this reduces to

$$\sigma(\mathbf{k}) = \pm \frac{k_z}{k} , \tag{9}$$

where $\pm$ corresponds to the $\pm$ in the field-aligned dispersion equation (1). If $\sigma(\mathbf{k}) = +1$, the wave fields exhibit a left-hand sense of rotation with respect to $\mathbf{k}$, while $\sigma(\mathbf{k}) = -1$ implies a right-handed field structure (Smith *et al.*, 1983). To avoid confusion with right- and left-hand polarizations, we will use the terms positive and negative helicities, respectively, to describe such fluctuations.

Figure 1 illustrates some differences between polarization and helicity. At frequencies below the proton-cyclotron frequency, the right-travelling magnetosonic/whistler and the left-travelling Alfvén/ion cyclotron waves have positive helicity at $\mathbf{k} \parallel \mathbf{B}_0$, whereas the left-travelling magnetosonic/whistler and the right-travelling Alfvén/ion cyclotron waves have negative helicity for the same wave vectors. In contrast, use of Equation (4) shows that the magnetosonic/whistler wave is right-hand circularly polarized, whatever its direction of propagation, whereas the Alfvén/ion cyclotron mode is left-hand circularly polarized for both left- and right-travelling waves.

In the next section of this paper we examine numerical solutions of the full electromagnetic dispersion equation in a homogeneous plasma derived from the complete set

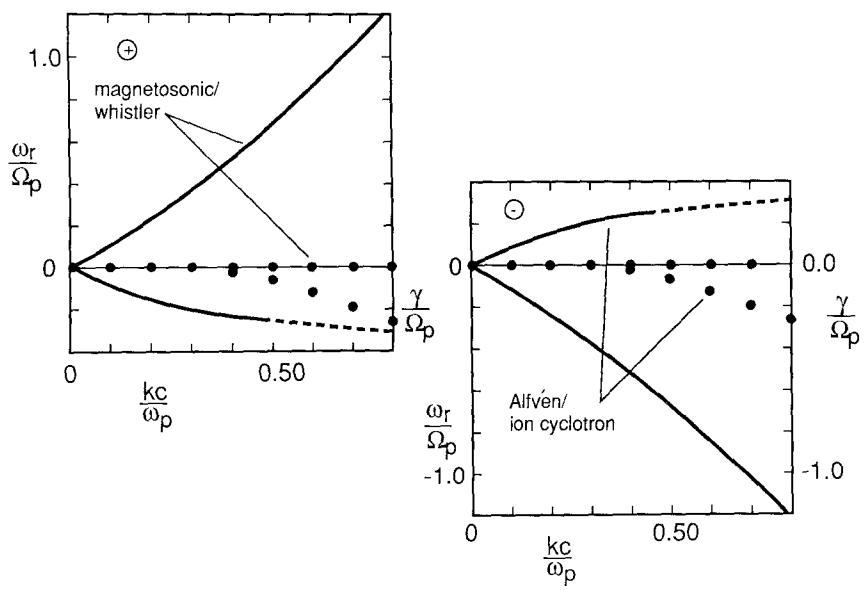

Fig. 1. The real frequency (solid lines and dashed lines) and damping rates (dotted lines) of low frequency waves as functions of wave number for positive helicity (left panel) and negative helicity (right panel). In both panels, the magnetosonic/whistler wave corresponds to the lightly damped mode which extends to $\Omega_p < |\omega_r|$, whereas the Alfvén/ion cyclotron wave corresponds to the more heavily damped mode which remains at $|\omega_r| < \Omega_p$ for all wave numbers shown. Plasma parameters are those given in Table I(a). Here $\theta = 0°$.

of Maxwell's equations and the linear Vlasov equation. If the zeroth-order distribution function for the jth component is a drifting Maxwellian, then

$$f_j^{(M)}(\mathbf{v} - \mathbf{v}_{0j}) = \frac{n_j}{(2\pi v_j^2)^{3/2}} \exp\left[- \frac{(\mathbf{v} - \mathbf{v}_{0j})^2}{2v_j^2} \right]. \tag{10}$$

The derivation of the electromagnetic dispersion equation based on this distribution for an arbitrary direction of $\mathbf{k}$ is well known (Stix, 1962) and is summarized in the Appendix.

If the zeroth-order distribution function of the jth component is a drifting bi-Maxwellian as discussed in Section 4.4,

$$f_j^{(0)}(\mathbf{v}) = \frac{n_j T_{\|j}}{(2\pi v_j^2)^{3/2} T_{\perp j}} \exp\left[- \frac{(v_z - v_{0j})^2}{2v_j^2} - \frac{v_\perp^2}{2v_j^2} \frac{T_{\|j}}{T_{\perp j}} \right], \tag{11}$$

then the corresponding dimensionless conductivity of that component at $\mathbf{k} \times \mathbf{B}_0 = 0$ is

$$S_j^{\pm}(\mathbf{k}, \omega) = \frac{\omega_j^2}{k^2 c^2} \left[\zeta_j Z(\zeta_j^{\pm}) + \left(1 - \frac{T_{\perp j}}{T_{\|j}} \right) \frac{Z'(\zeta_j^{\pm})}{2} \right], \tag{12}$$

where

$$\zeta_j \equiv \frac{(\omega - \mathbf{k} \cdot \mathbf{v}_{0j})}{\sqrt{2}\,|k_z|\, v_j} \quad \text{and} \quad \zeta_j^{\pm} \equiv \frac{(\omega - \mathbf{k} \cdot \mathbf{v}_{0j} \pm \Omega_j)}{\sqrt{2}\,|k_z|\, v_j} . \tag{13}$$

To model the full shell distributions discussed in Section 4.5, Gary and Sinha (1989) used distributions of the form

$$f_s^{(0)}(\mathbf{v}) = \frac{2^n n!}{(2n+1)!} \left(\frac{(\mathbf{v} - \mathbf{v}_{0s})^2}{v_s^2} \right)^n f_s^{(M)}(\mathbf{v} - \mathbf{v}_{0s}), \tag{14}$$

which implies a dimensionless conductivity at $\mathbf{k} \times \mathbf{B}_0 = 0$

$$S_s^{\pm}(\mathbf{k}, \omega) = \frac{\omega_s^2}{k^2 c^2} \zeta_s \frac{(2^n n!)^2}{(2n+1)!} \times$$

$$\times \left[Z(\zeta_s^{\pm}) \sum_{m=0}^{n} \frac{(\zeta_s^{\pm})^{2m}}{m!} + \frac{1}{\zeta_s^{\pm}} \sum_{m=1}^{n} \frac{(\zeta_s^{\pm})^{2m}}{m!} \sum_{l=0}^{m-1} \frac{1}{(\zeta_s^{\pm})^{2l}} \frac{(2l)!}{2^{2l} l!} \right], \tag{15}$$

with ζ_s and $\zeta_s^{\pm}$ defined as in Equation (13).

4. Linear Theory: Results

As has been discussed in Section 2, there are many different space plasma regimes in which two or more distinct ion components are observed or are inferred to stream relative to each other. These regimes correspond to quite diverse plasma parameters and, when the relative streaming speed is approximately greater than v_A, to several

distinct electromagnetic ion/ion instabilities. In this section we state average parameters for several of these regimes and discuss some of the linear properties of the instabilities which result.

Specificially, this section considers the linear theory of low-frequency waves and electromagnetic ion/ion instabilities in a homogeneous, magnetized Vlasov plasma. Although ion beam distributions can lead to instabilities well above the proton-cyclotron frequency, these higher frequency modes are usually associated with electron/ion relative drifts (Akimoto *et al.*, 1987), and usually attain a much lower peak amplitude than the corresponding ion/ion instabilities (Winske *et al.*, 1985a). Therefore, we here address only instabilities at $\omega_r \lesssim \Omega_p$. Furthermore, though there is an extensive literature describing analytic solutions of the electromagnetic dispersion equation for ion/ion instabilities, in this review we concentrate on results based on the more accurate procedure of computer solutions of the full Vlasov dispersion equation for a non-zero β plasma.

In this review we frequently use the terms 'resonant' and 'nonresonant'. An individual charged particle of species j is resonant with a wave or field fluctuation if its magnetic-field-aligned component of velocity v_z approximately satisfies the Landau ($\omega_r - k_z v_z = 0$) or the cyclotron ($\omega_r - k_z v_z \pm m\Omega_j = 0$ with $m = 1, 2, \ldots$) resonance condition. These conditions correspond to situations in which the particle sees a constant electric field in its own frame of reference, so that it can exchange a significant amount of energy with the wave.

If the jth component of the distribution function has an average velocity $\mathbf{v}_{0j}$ parallel or antiparallel to $\mathbf{B}_0$, and that component is cool in the sense that $v_j \ll v_{0j}$, then the cyclotron resonance condition for that component is

$$\omega_r - \mathbf{k} \cdot \mathbf{v}_{0j} \pm m\Omega_j = 0\,, \quad m = 1, 2, 3, \ldots\,, \tag{16}$$

where only the $m = \pm 1$ resonances contribute at $\mathbf{k} \times \mathbf{B}_0 = 0$, and where $m = \pm 1$ refers to the two helicity choices discussed under Equation (2). However, many electron and ion components observed in space plasmas are not cool but warm in the sense that their thermal speeds are of the same order as their drift speeds ($v_j \sim v_{0j}$). Such components, as well as hot components ith ($v_j \gg v_{0j}$), may also have a significant number of particles which have a strong wave-particle resonance. This will be the case if the resonant velocity lies within a thermal speed of the peak of the distribution function, so that at parallel propagation the component is Landau or cyclotron resonant if, at $\mathbf{k} \times \mathbf{B}_0 = 0$,

$$|\zeta_j| \lesssim 1 \quad \text{or} \quad |\zeta_j^{\pm}| \lesssim 1\,, \tag{17}$$

respectively, where ζ_j and $\zeta_j^{\pm}$ are defined as in Equation (13). (For the more general case of oblique propagation, the mth cyclotron resonance condition is $|\zeta_j^m| \lesssim 1$, where ζ_j^m is defined in the Appendix.) In the opposite case,

$$|\zeta_j| \gg 1 \quad \text{or} \quad |\zeta_j^{\pm}| \gg 1\,, \tag{18}$$

all component particles experience relatively weak wave-particle interactions during the

small amplitude, linear phase of an instability and the component is termed 'nonresonant' with respect to that growing mode.

In each of the following subsections, we consider the plasma to consist of a single Maxwellian electron component and one or two proton components. Dimensionless parameters which represent some of the proton component models considered here are given in Table I. Use of these parameters in the linear dispersion equation leads to the growth of several different instabilities with maximum growth rates at $\mathbf{k} \times \mathbf{B}_0 = 0$.

Properties of those instabilities which we regard as most important are summarized in Table II. Our rationale for the nomenclature used here is as follows: Because of severe changes in dispersion which arise as v_0/v_A becomes much greater than unity, we use the terms 'ion/ion right-hand resonant' and 'ion/ion left-hand resonant' for the two modes which approximately satisfy $|\zeta_b^{\pm}| \lesssim 1$, and 'nonresonant' for the $|\zeta_b^{\pm}| \gg 1$ fluid-like instability in this configuration. This represents two changes from the names chosen by Gary *et al.* (1984): Instead of 'ion beam', we use the more complete term 'ion/ion' to describe the free energy driving these modes, and we drop the adjective 'right-hand' from the nonresonant instability because its very low frequency corresponds to a change in polarization between the center of mass and solar wind frames, thereby removing polarization as a useful identifier for this mode. Representative ion distribution functions and the corresponding cyclotron resonant speeds for four of the instabilities of Table II are illustrated in Figure 2.

4.1. Maxwellian proton core

We first consider the case in which each species consists of a single component, protons and electrons, with $T_p \simeq T_e$. Then there are two weakly damped normal modes of the plasma at $\omega_r \lesssim \Omega_p$. The magnetosonic/whistler mode is the wave of right-hand circular polarization at $\mathbf{k} \times \mathbf{B}_0 = 0$, and has neither resonance nor cutoff over $0 < \omega_r \lesssim \Omega_p$. The Alfvén/ion cyclotron mode has left-hand circular polarization at $\mathbf{k} \times \mathbf{B}_0$, and goes to an ion-cyclotron resonance which increases its ion cyclotron damping at short wavelengths and limits its propagation to $0 < \omega_r \ll \Omega_p$ (see Figure 1).

Barnes (1966) used numerical solutions of the dispersion equation at $\omega_r \ll \Omega_p$ to study the damping of the magnetosonic mode at arbitrary wavevector angle θ. In particular, Barnes demonstrated that this damping increased as the plasma β increased. Gary (1986) extended this work to $\omega_r \lesssim \Omega_p$ and to the Alfvén/ion cyclotron mode, as well as examining the polarization, helicity and compressibility of both modes as a function of wave number and propagation angle. Figure 3 elaborates several of the results of Gary (1986), showing that, at a fixed wave number, the polarization of both modes approaches the linear condition and the dimensionless helicity becomes quite small as propagation becomes strongly oblique. Figure 4 of Brinca and Tsurutani (1987b) shows similar results for the polarizations of both modes at somewhat lower β_c and longer wavelengths.

TABLE I

Dimensionless plasma parameters
$v_A/c = 1.0 \times 10^{-4}$

(a) Maxwellian proton core

		Protons	Electrons
Mass	m_j/m_e	1836	1
Density	n_j/n_e	1.00	1.00
Flow speed	v_{0j}/v_A	0.00	0.00
Temperature	T_j/T_p	1.00	1.00
Anisotropy	$T_{\perp j}/T_{\parallel j}$	1.00	1.00
Beta	$\beta_j = 8\pi n_e T_j/B_0^2$	1.00	1.00

(b) Proton core with hot proton beam

		Core	Beam	Electrons
Mass	m_j/m_e	1836	1836	1
Density	n_j/n_e	0.99	0.01	1.00
Flow speed	v_{0j}/v_A	−0.02	+1.98	0.00
Temperature	T_j/T_c	1.00	100.00	1.00
Anisotropy	$T_{\perp j}/T_{\parallel j}$	1.00	1.00	1.00
Core beta	$\beta_c = 8\pi n_e T_c/B_0^2$	1.00		

(c) Proton core with cool proton beam

		Core	Beam	Electrons
Mass	m_j/m_e	1836	1836	1
Density	n_j/n_e	0.99	0.01	1.00
Flow speed	v_{0j}/v_A	−0.08	+7.92	0.00
Temperature	T_j/T_c	1.00	10.00	1.00
Anisotropy	$T_{\perp j}/T_{\parallel j}$	1.00	1.00	1.00
Core beta	$\beta_c = 8\pi n_e T_c/B_0^2$	1.00		

(d) Anisotropic proton core with proton beam

		Core	Beam	Electrons
Mass	m_j/m_e	1836	1836	1
Density	n_j/n_e	0.80	0.20	1.00
Flow speed	v_{0j}/v_A	∓ 0.20	± 0.80	0.00
Temperature	T_j/T_c	1.00	1.00	1.00
Anisotropy	$T_{\perp j}/T_{\parallel j}$	10.00	1.00	1.00
Core beta	$\beta_c = 8\pi n_e T_c/B_0^2$	1.00		

(e) Proton core with proton shell

		Core	Shell	Electrons
Mass	m_j/m_e	1836	1836	1
Density	n_j/n_e	0.99	0.01	1.00
Flow speed	v_{0j}/v_A	−0.02	+1.98	0.00
Temperature	T_j/T_c	1.00		1.00
Anisotropy	$T_{\perp j}/T_{\parallel j}$	1.00	1.00	1.00
Core beta	$\beta_c = 8\pi n_e T_c/B_0^2$	1.00		

TABLE II

Five electromagnetic instabilities at $\mathbf{k} \times \mathbf{B}_0 = 0$

Name	Frequencies, center of mass polariztion	Parameter regimes	Other names	Recent references
Ion/ion right-hand resonant	$\omega_r \ll \Omega_p$, *right-hand*	$v_A \lesssim v_0$ and very small n_b/n_e	'magnetosonic' 'fast MHD' B&T:RFxS	Gary *et al.* (1985)
Ion/ion nonresonant	$\omega_r \simeq 0$, varies	$v_A \ll v_0$ or modest n_b/n_e	'firehose' B&T:LFNR	Winske and Gary (1986)
Ion/ion left-hand resonant	$\omega_r \ll \Omega_p$, *left-hand*	Warm or hot beam and $v_A \lesssim v_0$	'Alfvén'	Gary (1985)
Ion cyclotron anisotropy	$\omega_r < \Omega_p$, left-hand	$T_{\parallel b} < T_{\perp b}$	B&T:LFxS and LBxS	Gary and Schriver (1987) Gary and Madland (1988)
Electron/ion whistler	$\Omega_p < \omega_r$, right-hand	$v_A \ll v_0$	B&T:RFxH	Akimoto *et al.* (1987)

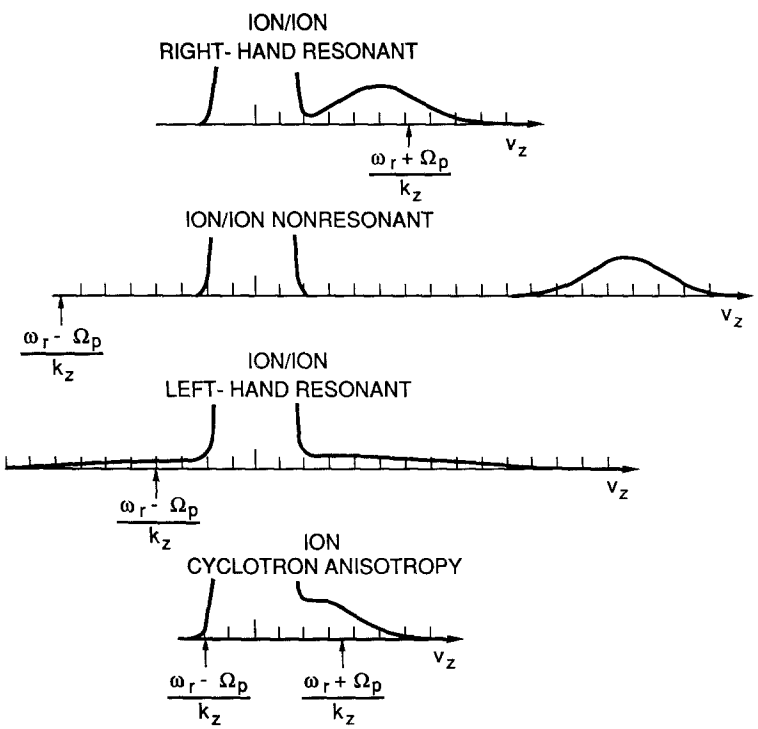

Fig. 2. Reduced ion distribution functions corresponding to four of the $\mathbf{k} \times \mathbf{B}_0 = 0$ instabilities of Table II, and the associated proton cyclotron resonant speeds (after Figure 1 of Gary and Tokar, 1985).

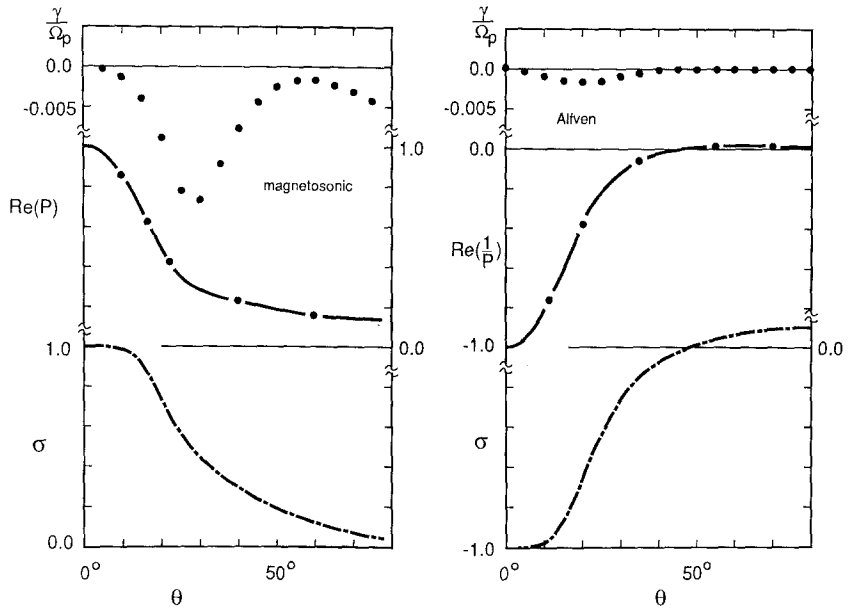

Fig. 3. The damping rate (dotted lines), the real part of the polarization or reciprocal of the polarization (dashed-dot lines), and the dimensionless helicity (long dash-short dash lines) as functions of the propagation angle for the magnetosonic (left panel) and Alfvén (right panel) modes at $kc/\omega_p = 0.12$. Plasma parameters are those given in Table I(a).

4.2. Proton Core with a Maxwellian Proton Beam

In this subsection we consider the ions to consist of two drifting Maxwellian components, a proton core and a more tenuous proton beam. Each component is isotropic in its own frame. The fully electromagnetic dispersion equation described in the Appendix is the appropriate theory here. In this model, it is useful to define three distinct beam regimes: we term a 'cool' beam one which satisfies $0 < v_b \ll v_{0b}$, a 'warm' beam satisfies $v_{0b} \sim v_b$, and if $v_{0b} \ll v_b$, we term the beam 'hot'.

Sentman *et al.* (1981) and Gary (1985) examined linear instability theory for hot, tenuous ion beams similar to the 'diffuse' ions of the terrestrial foreshock and the energetic ion component observed in the environment of interplanetary shocks. These papers demonstrated the following properties for electromagnetic ion/ion instabilities if both ion components are hot and isotropic: As v_0 is increased from zero, both the right-hand polarized magnetosonic/whistler and the left-hand polarized Alfvén/ion cyclotron modes experience a reduction in damping until near $v_0 \sim v_A$, the beam/core relative drift exceeds the threshold for wave growth with $\gamma > 0$ first appearing at $\mathbf{k} \times \mathbf{B}_0 = 0$.

As long as the hot beam condition $v_{0b} \ll v_b$, is satisfied, several wave properties of both right- and leftr-hand modes are not significantly altered, even above instability threshold. These properties include not only the dispersion $\omega_r(k)$, but also the polarization and helicity as a function of propagation angle θ. Figure 4 displays these latter

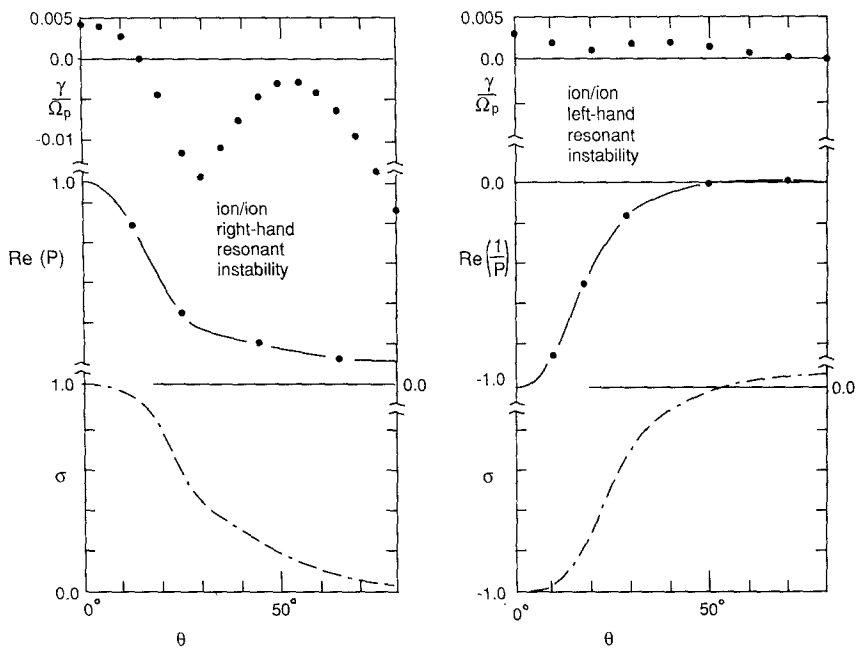

Fig. 4. The growth and damping rates (dotted line), the real part of the polarization or reciprocal of the polarization (dashed-dot line), and the dimensionless helicity (long dash-short dash line) as functions of propagation angle for two instabilities at $kc/\omega_p = 0.12$. The left-hand panel represents the ion/ion right-hand resonant instability for the parameters of Table I(b); panel (b) illustrates the ion/ion left-hand resonant instability for the same parameters.

two quantities at $v_0 = 2v_A$, which are essentially unchanged from the single proton component case of Figure 3. Figure 3 of Hada *et al.* (1987) illustrates the density compression ratio and the magnetic field compression ratio for the right-hand resonant instability in the presence of a diffuse ion beam distribution.

As the beam temperature is reduced so that this ion component becomes merely warm, there are fewer ions moving antiparallel to $\mathbf{v}_0$, and, as Figure 2 suggests, the growth rate of the ion/ion left-hand resonant instability decreases. The linear dispersion theory of this regime has been studied for solar wind parameters by Montgomery *et al.* (1975, 1976), Lakhina and Buti (1976), Gary (1978b), Abraham-Shrauner *et al.* (1979), Dum *et al.* (1980), and Leubner and Vinãs (1986). An extensive study of warm ion beams observed in the solar wind between 0.3 and 1 AU has been carried out by Marsch and Livi (1987). Their analysis of several thousand ion spectra showed that these distributions are often unstable to the right-hand resonant instability and, on rare occasions when n_b/n_e is sufficiently large, are also unstable to the nonresonant mode. In the high-speed solar wind a large number of unstable distributions were found, but the average value of v_0/v_A remained not far above the stability boundary in most cases.

Oblique propagation for warm ion beams similar to those observed in the solar wind was examined by Montgomery *et al.* (1976), who found γ_m at $\theta = 0°$ for almost all of

the parameter space they surveyed. Similarly, the oblique growth rates obtained by Gary (1985) for the hot ion beam case were always smaller than those at $\mathbf{k} \times \mathbf{B}_0 = 0$.

The computer simulations of Winske *et al.* (1985b) showed that warm ion beams at $v_0 \sim 2v_A$ can arise upstream of slow shocks such as those found in the deep magnetotail (Feldman *et al.*, 1985, and references therein). Gary *et al.* (1985) showed that this low v_0 condition, especially when coupled with the low β_c condition of the deep tail boundary layer, implied that the right-hand resonant instability should have maximum growth rate at $\omega_r \lesssim \Omega_p$.

In the cool beam regime, there are very few particles moving in the direction anti-parallel to $\mathbf{v}_0$; since it is these ions which drive the ion/ion left-hand resonant instability (see Figure 2), the growth rate of this mode is eventually diminished as the core/beam relative drift increases (Gary *et al.*, 1984). However, the ion/ion right-hand resonant instability persists, as was early demonstrated by Barnes (1970), because ω_r satisfies Equation (16) and the mode remains resonant no matter how large the beam/core relative drift becomes. Gary (1978a) demonstrated that the dispersion of this instability was distinctly non-Alfvénic, and that the maximum growth rate at $v_A \ll v_0$ satisfies

$$\frac{\gamma_m}{\Omega_p} \simeq \left(\frac{n_b}{2n_e}\right)^{1/3} . \tag{19}$$

Sentman *et al.* (1981) showed that a cool fast ion beam can also excite a nonresonant, firehose-like instability which, unlike the resonant modes, propagates in the direction opposite to the beam, and has a cyclotron resonance speed which lies far from either ion component (see Figure 2). Gary *et al.* (1984) demonstrated that the resonant mode typically has the lower threshold v_0, but that the nonresonant mode can have the larger growth rate if v_0/v_A and n_b/n_e are sufficiently large. This last point is clear by comparing Equation (19) with the Winske and Leroy (1984) expression for the maximum growth rate of the ion/ion nonresonant instability at $n_b \ll n_e$ and $v_0 \ll v_A$:

$$\frac{\gamma_m}{\Omega_p} \simeq \frac{n_b}{2n_e} \frac{v_0}{v_A} . \tag{20}$$

Gary *et al.* (1986a) used linear theory at $\theta = 0°$ to derive an expression for the phase angle between the fluctuating magnetic field of an instability and the fluctuating velocity vector of each plasma component. They also showed that the right-hand resonant mode is the more likely cool ion beam instability to cause observable phase bunching of the beam during linear instability growth.

Gary *et al.* (1981) considered oblique propagation of the ion/ion right-hand resonant instability and showed that, although the instability exhibited strong compressibility at relatively small angles of propagation relative to $\mathbf{B}_0$, the maximum growth rate remained at $\theta = 0°$. Although γ_m typically remains at $\mathbf{k} \times \mathbf{B}_0 = 0$ for both the right-hand resonant and nonresonant instabilities (e.g., Gary *et al.*, 1984; Hada *et al.*, 1987), growth rates at oblique propagation can be significant for both modes. And since finite plasma effects as well as wave refraction (Hada *et al.*, 1987) can impose a nonzero perpendicular

component of the wave number, studies of instability properties at $\theta \neq 0$ remain appropriate. In particular, Goldstein *et al.* (1983) demonstrated that both right-hand and left-hand instabilities at oblique propagation can manifest relative maxima in the γ vs k_z plots corresponding to the $2 \leq |m|$ resonances of Equation (16).

As v_{0b}/v_b becomes much greater than unity, not only does $\omega_r(k)$ develop strong differences with respect to its zero drift properties, but so also do the polarization and helicity at oblique propagation. In particular, the polarization remains relatively close to unity for comparatively large values of θ (Gary and Winske, 1986) for both the right-hand resonant and nonresonant instabilities, as shown in Figure 5. Figure 6 illustrates some further properties of these two growing modes at oblique propagation. The top panel of both parts (a) and (b) shows the growth rate as a function of θ; the resonant mode can persist with significant growth to much more oblique angles than its nonresonant counterpart. The middle panels illustrate the real part of the polarization, P,

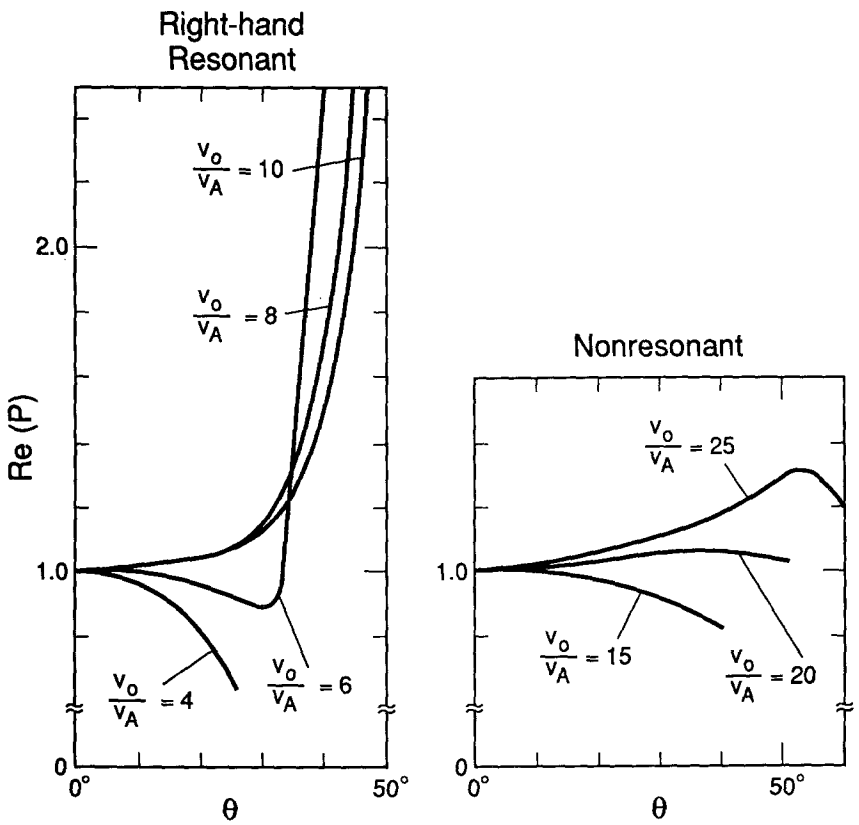

Fig. 5. The real part of the polarization for the ion/ion right-hand resonant and nonresonant instabilities as a function of propagation angle at the wavenumber of maximum growth rate. Parameters are those of Table I(c). In the left-hand panel, $v_0/v_A = 4$ corresponds to $kc/\omega_p = 0.24$; $v_0/v_A = 6$ corresponds to $kc/\omega_p = 0.16$; $v_0/v_A = 8$ corresponds to $kc/\omega_p = 0.12$; and $v_0/v_A = 10$ corresponds to $kc/\omega_p = 0.095$. In the right-hand panel, $v_0/v_A = 15$ corresponds to $kc/\omega_p = 0.05$; $v_0/v_A = 20$ corresponds to $kc/\omega_p = 0.085$; and $v_0/v_A = 25$ corresponds to $kc/\omega_p = 0.115$.

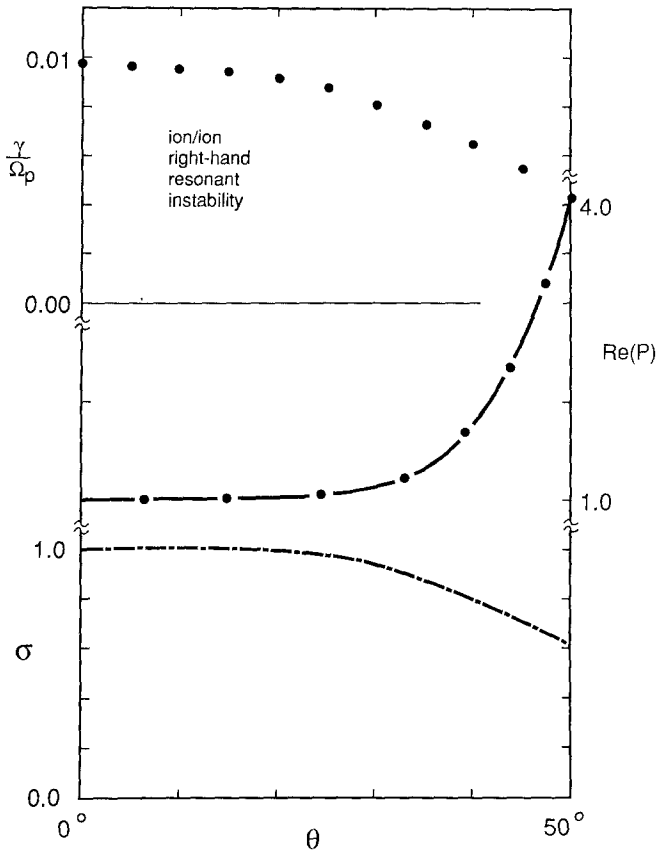
0.01
γ/Ωp
ion/ion
right-hand
resonant
instability
4.0
0.00
Re(P)
1.0
1.0
σ
0.0
0°
θ
50°

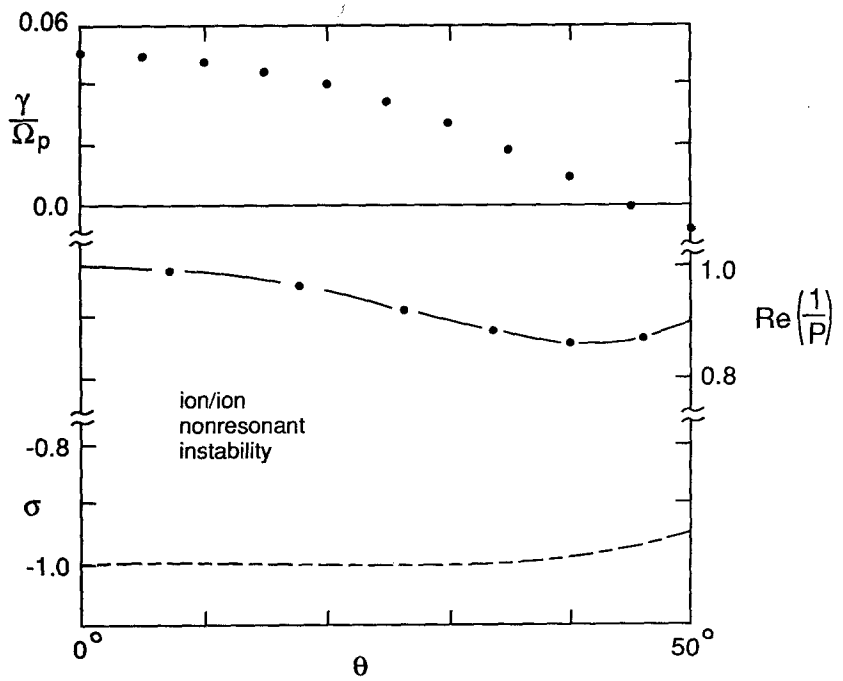
0.06
γ/Ωp
0.0
1.0
Re(1/P)
0.8
ion/ion
nonresonant
instability
-0.8
σ
-1.0
0°
θ
50°

or of the reciprocal of the polarization, $1/P$. For the case $v_0/v_A \gg 1$ considered here, both the resonant and the nonresonant modes remain approximately right-hand circular polarized for $\theta \lesssim 45°$ (see also Figure 1 of Gary and Winske (1986)). Note the contrast with Figure 3, in which there is a strong tendency to linear polarization as θ increases away from zero. The bottom panel in Figures 6(a) and 6(b) shows the dimensionless helicity for these two instabilities; again, in contrast to the result for a plasma with no ion beam present, the dimensionless helicity remains near the value ± 1 for $\theta \lesssim 45°$.

The relationship between the two resonant instabilities is illustrated in Figure 7, which plots the maximum growth rate for both as a function of core β. At $\beta_c = 1.0$, where the parameters of Table I(b) correspond to those of a hot beam, γ_m of the two modes is of the same order of magnitude (Gary, 1985). As β_c is decreased, if all other parameters of Table I(b) are held constant, v_0/v_b decreases, so that at $\beta_c = 0.08$, the warm beam condition $v_0 = v_b$ is satisfied, and at $\beta_c \simeq 0.01$, the distribution enters the cool beam regime, $v_b \ll v_0$. As the core β undergoes this decrease, the maximum growth rate of the

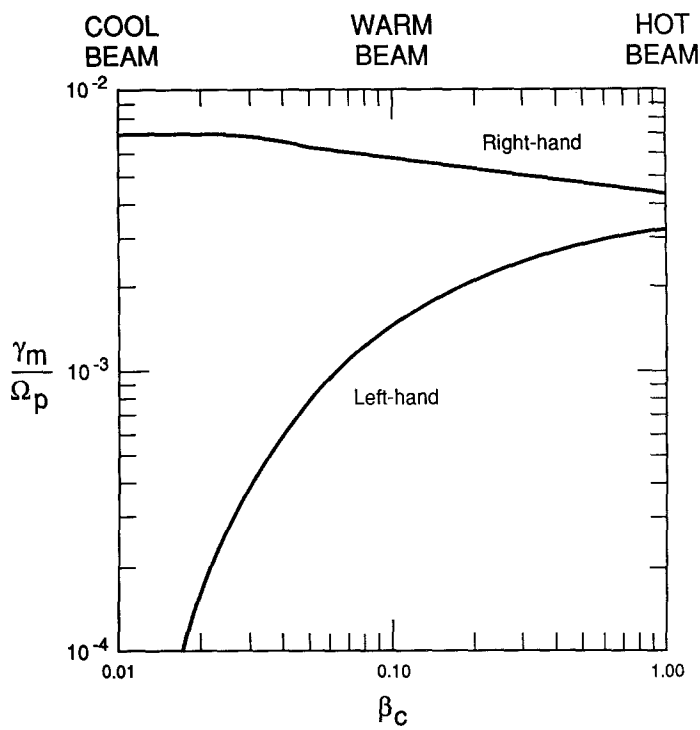

Fig. 7. The maximum growth rate for the two ion/ion resonant instabilities as a function of β_c. The parameters are those of Table I(b) except for β_c. Here $\theta = 0°$.

◀ Fig. 6. The growth rate (dotted line), the real part of the polarization or reciprocal of the polarization (dashed-dot line), and the dimensionless helicity (long dash-short dash line) as functions of propagation angle for two instabilities at $kc/\omega_p = 0.12$. Panel (a) represents the ion/ion right-hand resonant instability for the parameters of Table I(c); panel (b) illustrates the ion/ion nonresonant instability for the parameters of Table I(c) except that $v_0 = 20v_A$.

right-hand resonant mode increases somewhat, but γ_m of the left-hand resonant mode decreases.

We can provide a physical interpretation of these results by considering the $\mathbf{k} \times \mathbf{B}_0 = 0$ dispersion equation (1). If we assume that the beam distribution function is isotropic in its own frame, then the conductivity of Equation (2) reduces to a single term under the integral. If we then cast the proton core and electron terms in the form of Equation (8 ±) of Gary (1985) by using the nonresonant properties of these two components and assuming $|k_z v_{0c}| \ll \omega_r \ll \Omega_p$, then by further assuming $|\gamma| \ll \omega_r$ it follows that

$$\gamma \simeq \frac{2\pi^2 \omega_b^2 \omega_r (v_{0b} - \omega/k_z)}{n_b \left(|\omega|^2 + |\omega|^2 \frac{\omega_c^2}{\Omega_p^2} + k^2 c^2 \right)} \int_0^\infty \mathrm{d}v_\perp v_\perp f_b^{(0)}(v)|_{v_z = (\omega \pm \Omega_p)/k_z} . \tag{21}$$

Since both right-hand and left-hand resonant instabilities propagate in the same direction as the ion beam, $v_{0b}\omega_r > 0$, and it follows that the threshold instability criterion for both growing modes is $v_{0b} > \omega_r/k_z \simeq v_A$. And since the growth rate is proportional to the velocity-space density of beam particles in resonance with the wave, it follows that the cooler the beam, the greater should be the growth rate of the right-hand resonant instability, and the smaller should be the γ of the left-hand resonant instability, as indeed is shown in Figure 7.

4.3. Proton core with a Maxwellian heavy ion beam

Winske and Gary (1986) studied the properties of electromagnetic ion/ion instabilities driven by cool heavy beams. They demonstrated that, whereas γ_m of the nonresonant instability (Equation (20)) is essentially independent of m_b/m_p, the maximum growth rate of the right-hand resonant instability at $v_A \ll v_0$ scales as

$$\frac{\gamma_m}{\Omega_p} \simeq \left(\frac{n_b}{2n_e} \right)^{1/3} \left(\frac{m_p}{m_b} \right)^{2/3} . \tag{22}$$

Thus, although the right-hand resonant instability retains the lower threshold and larger growth rate for very tenuous, relatively slow heavy beams, the ion/ion nonresonant instability can become the faster growing mode more readily if the beam is composed of heavy ions. Goldstein and Wong (1987) also examined the generation of the nonresonant instability by a relatively cold heavy ion beam, and concluded that it was competitive with the right-hand resonant instability for a sufficiently large density of cometary oxygen ions in the Giacobini–Zinner environment.

If two cool, tenuous beams are present with disparate masses, such as newborn protons and water-group ions in a cometary environment, two distinct branches of the right-hand resonant instability may arise (Gary and Madland, 1988; Brinca and Tsurutani, 1988). The proton/proton instability has frequencies and growth rates that scale with Ω_p, whereas the heavy-ion/proton instability has ω_r- and γ-values that scale

with the heavy ion-cyclotron frequency. Thus the former mode has much higher frequencies, much faster growth rates, and, by Equation (16), much shorter wavelengths than the latter instability. This substantial wavelength and frequency separation implies that the two modes should evolve independently during linear growth, and the computer simulations of Gary *et al.* (1988) have demonstrated that this is indeed the case.

4.4. Anisotropic proton core or anisotropic ion beam

In this subsection, one of the two ion components is taken to be an anisotropic bi-Maxwellian (Equation (11)) with the corresponding conductivity at $\mathbf{k} \times \mathbf{B}_0 = 0$ given by Equation (12). If $v_0 = 0$, this component anisotropy can drive the electromagnetic ion-cyclotron anisotropy instability (Davidson and Ogden, 1975) which is left-hand polarized and propagates both parallel and antiparallel to $\mathbf{B}_0$. This instability has numerous applications to space physics under both $v_0 = 0$ and $v_0 \neq 0$. This review addresses only the latter case; the linear theory of zero-drift configurations has been reviewed by several authors including Cuperman (1981) and Gendrin *et al.* (1984).

In the configuration consisting of an ion core plus an ion beam a sufficiently large anisotropy of either component can permit this instability to grow. Although this mode exhibits Alfvénic dispersion at long wavelengths, it is ion cyclotron resonant (i.e., $|\zeta_i^{\pm}| \lesssim 1$), it does not have significant growth at $kc/\omega_p \ll 1$, and is typically not unstable in the regime of Alfvénic dispersion (see Figures 2 and 3 of Davidson and Ogden, 1975). Moreover, if the ion core bears a sufficiently strong anisotropy, the long wavelength dispersion of the instability is not Alfvén-like at all, but rather ω_r approaches Ω_p as the wave number goes to zero (Angelopoulos *et al.*, 1989). Thus the term 'Alfvén/ ion-cyclotron instability' is not appropriate for this mode.

Gary and Schriver (1987) examined the response of the maximum growth rate for an anisotropic beam as v_0 is increased from zero. They showed that a nonzero beam/core relative drift favors that branch of the left-hand polarized instability which propagates antiparallel to the beam, although as v_0/v_A increases above unity, $\omega_r(k)$ of this branch becomes strongly Doppler shifted at short wavelengths and becomes the ion/ion right-hand resonant instability propagating parallel to the beam. Thus as v_0/v_b becomes sufficiently large, left-hand instabilities are suppressed (Figures 4 and 5 of Gary and Schriver, 1987). And in the cool beam, high drift speed limit of $v_b \ll v_0$, $T_{\parallel b} \ll T_{\perp b}$ has essentially no effect on the ion/ion nonresonant instability, and implies a modest increase in the maximum growth rate of the right-hand resonant instability (Figure 6 of Gary *et al.*, 1984).

If v_0/v_A is held fixed and $T_{\perp b}/T_{\parallel b}$ is increased from unity, the maximum growth rates of both the (left-hand) ion-cyclotron anisotropy instability and the ion/ion left-hand resonant instability are enhanced, whereas γ_m of the ion/ion right-hand resonant instability is reduced (Figure 7 of Montgomery *et al.*, 1976; Figure 6 of Gary, 1985). Brinca and Tsurutani (1988) have surveyed the linear dispersion properties of electromagnetic instabilities driven by a relatively cold, anisotropic ion beam and have stated a novel instability notation to describe the various growing modes. We have related our terminology to some of their identifiers (labeled B&T) in the fourth column of Table II.

At propagation oblique to $\mathbf{B}_0$, Smith and Gary (1987) showed that $T_{\perp b} > T_{\parallel b}$, as well as increasing beam density and core/beam drift speed, enhances the growth rates at the $|m| > 1$ cyclotron resonances for both right- and left-hand polarized modes. However, although Brinca and Tsurutani (1989a) showed that an anisotropic ion beam could excite relative maxima in growth rate contours as a function of k_y and k_z, neither they nor Smith and Gary (1987) were able to exhibit specific examples in which the growth rate at $\theta > 0$ was greater than or even equal to the maximum growth rate at $\mathbf{k} \times \mathbf{B}_0 = 0$.

If it is the ion core which exhibits the temperature anisotropy, modest increases in $T_{\perp c}/T_{\parallel c}$ above unity reduce γ_m of both ion/ion resonant modes (Figure 7, Montgomery *et al.*, 1976). If $T_{\perp c}/T_{\parallel c}$ becomes sufficiently large at fixed v_0/v_A, the right-hand instability changes the sign of frequency, its polarization, and its direction of propagation, so that the ion cyclotron anisotropy instability can once again grow with left-hand polarization in both directions relative to $\mathbf{B}_0$. Figure 8 illustrates some representative dispersion properties of this mode: as with its beam-driven counterpart, $v_0 \sim v_A$ enhances the branch propagating antiparallel to the anisotropic component. The parallel propagating branch is less unstable, but, by virtue of a strong Doppler shift, yields significant linear growth at $\omega_r > \Omega_p$ (Angelopoulos *et al.*, 1989).

4.5. Proton Core with an Ion Ring-Beam

If a tenuous neutral gas in the solar wind is ionized, say, by solar photoionization, the newborn ions initially assume a cold ring-beam distribution with pitch-angle α, the angle between the solar wind velocity $\mathbf{v}_{sw}$ and the interplanetary magnetic field $\mathbf{B}_0$. Electromagnetic instabilities driven by such a distribution were first studied by Wu and Davidson (1972) and Wu and Hartle (1974) who analytically showed that this con-

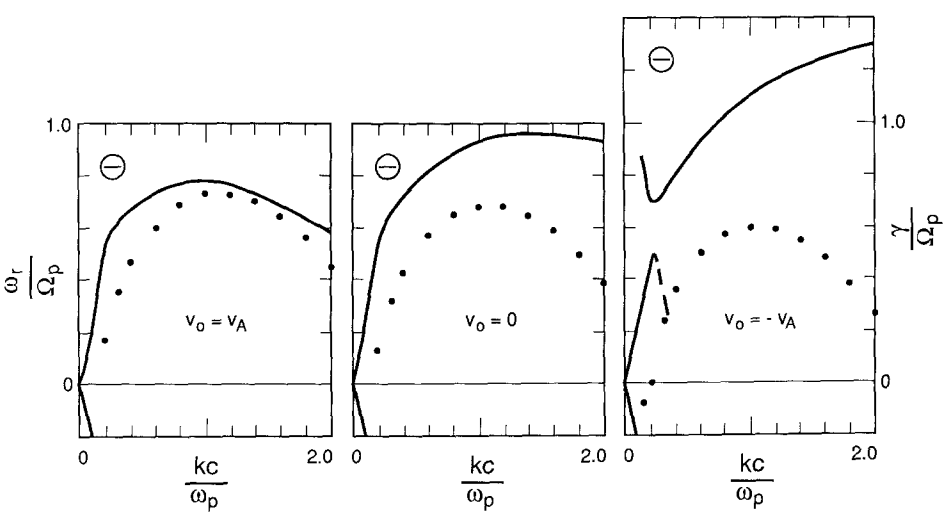

Fig. 8. The real frequency (solid lines and dashed lines) and growth rates (dotted lines) of negative helicity fluctuations as functions of wave number at $v_0 = v_A, 0$ and $-v_A$. In each panel, the growth rates correspond to the mode of most positive ω_r, the ion-cyclotron anisotropy instability; the damping rates of the other modes are not shown. Plasma parameters are those given in Table I(d). Here $\theta = 0°$.

figuration could drive three instabilities: a whistler resonant mode, another resonant mode at $\omega_r \ll \Omega_p$, and a fluid 'garden hose' instability (using the terminology of Table II, we call these the electron/ion whistler, the ion/ion right-hand resonant and the ion/ion nonresonant instabilities).

Winske *et al.* (1984, 1985a) numerically solved the linear dispersion equation in the cold ion ring-beam case and in particular showed that the scalings of the maximum linear growth rate for both the resonant and nonresonant low-frequency instabilities at $\alpha \simeq 45°$ were very similar to the scalings of γ_m in the cold beam case of $\alpha = 0°$. Gary and Madland (1988) extended the linear dispersion analysis of the cold ring-beam to $\alpha = 90°$ and showed that, although a left-hand polarized instability arose as the tenuous ion component became more ring-like, the right-hand polarized instability had the larger growth rate at all α-values.

A serious problem with cold ring-beam distributions is that they have never been observed in space plasmas. In the cometary environment, for example, where one might expect ionization of neutrals to give rise to such distributions, cometary ions are observed to have nonzero widths in velocity space. This broadening, which may be due either to pitch-angle scattering by relatively short wavelength magnetic fluctuations or to pickup over a range of α angles due to relatively long wavelength fluctuations, implies significant changes in the properties of the unstable modes, especially near $\alpha = 90°$.

Gary and Madland (1988) and Freund and Wu (1988) have shown that velocity-space spreading of a cold ring or cold ring-beam significantly decreases the linear growth rate of the associated ion-cyclotron instabilities. After comparing various linear theory calculations, Gary *et al.* (1989) summarized the linear instability properties of a tenuous, warm ion ring-beam distribution as follows: at relatively small values of α, the ion/ion right-hand resonant instability is the fastest growing instability, with γ_m which gradually increases with increasing α. At sufficiently large values of α, left-hand ion-cyclotron anisotropy instabilities appear (Thorne and Tsurutani, 1987); their growth rates also increase as α increases (Brinca and Tsurutani, 1987b, 1988; Gary and Madland, 1988). At even larger α, left-hand instabilities obtain the larger maximum growth rate; the precise angle at which this happens appears to depend on the model distribution, but typically is in the vicinity of the value $\alpha \simeq 75°$ quoted by Thorne and Tsurutani (1987). At $\alpha = 90°$, the left-hand ion-cyclotron instability is the only growing mode at $\mathbf{k} \times \mathbf{B}_0 = 0$.

Brinca and Tsurutani (1987a, b) considered the oblique propagation properties of low-frequency instabilities driven by a heavy ion beam with a loss-cone distribution, which has several properties similar to those of a thermally broadened ring-beam. They showed that the left-hand ion-cyclotron instability which arises at relatively large α can have a polarization which approaches linear at only slightly oblique propagation. Their numerical examples show linear polarization of this mode at $\theta \simeq 10°$, which stands in contrast to the much larger values for the θ values of linear polarization for the ion/ion instabilities illustrated in our Figures 4, 5, and 6. Brinca and Tsurutani (1987b) also demonstrated that loss-cone distributions of heavy ions can lead to maximum growth rates at small but oblique angles of propagation, and Brinca and Tsurutani (1989b) studied the excitation of cyclotron harmonics by such distributions.

4.6. Proton Core with a Shell Ion Component

If a cool, tenuous ion beam is pitch-angle scattered without significant energy change, its distribution evolves into a relatively complete shell distribution in velocity space. In this subsection, the electrons and ion core components are once again drifting Maxwellians, but the tenuous ion component is taken to be a complete shell distribution as in Equation (14) with Equation (15) the corresponding dimensionless conductivity at $\mathbf{k} \times \mathbf{B}_0 = 0$.

Freund and Wu (1988) used linear dispersion theory to show that complete ion shell distributions which are isotropic in the ion core frame are stable. Gary and Sinha (1989) showed that, if a complete ion shell has a sufficiently large drift speed relative to the ion core, the plasma is unstable to both the ion/ion right-hand and left-hand resonant instabilities, much as though the tenuous ion component were the hot Maxwellian beam of Section 4.2.

Figure 9 shows the dispersion plots (ω_r and γ vs k) for the ion/ion left-hand resonant instability for three similar conditions: a hot Maxwellian ion beam, a relatively broad ion shell distribution and a comparatively narrow ion shell distribution. Figure 3 of Gary and Sinha (1989) shows a similar result for the right-hand resonant instability: as the complete shell distribution becomes narrower in velocity space, the maximum growth rate of both modes increases. This result may be interpreted in terms of Equation (21), which applies to any ion beam distribution which is isotropic in its own frame. For the particular case of a drifting shell distribution, this equation implies that, as the shell becomes narrower and more ions come into resonance with the mode, γ_m increases.

5. Quasilinear Theories

In this section we review second-order and quasilinear theories of electromagnetic ion/ion instabilities. By 'second-order' we mean theories which use first-order fluctuating quantities to compute the slowly varying part of the second-order plasma response to instability growth. Such theories are limited to times before instability saturation, but can provide information about the approach to that condition if strongly nonlinear effects do not play a role. Quasilinear theories go a step beyond second order theories in that they fold the second order response back into the linear dispersion equation so that, if the fluctuating fields are sufficiently weak, they may be valid through saturation. A major disadvantage of quasilinear theories is that they often must utilize serious approximations in order to obtain a concise, tractible formalism.

A second-order formalism for $\mathbf{k} \times \mathbf{B}_0 = 0$ electromagnetic instabilities in a homogeneous plasma was developed by Gary and Feldman (1978), under the assumption that individual plasma components maintained near-Maxwellian properties and that the effect of wave-particle interactions could be expressed in terms of component flow speeds, temperatures and anisotropies. Applications of this theory to ion/ion instabilities have been pursued by Gary (1978a), Winske and Leroy (1984), Gary and Tokar (1985), Rogers *et al.* (1985), and Gaffey *et al.* (1988).

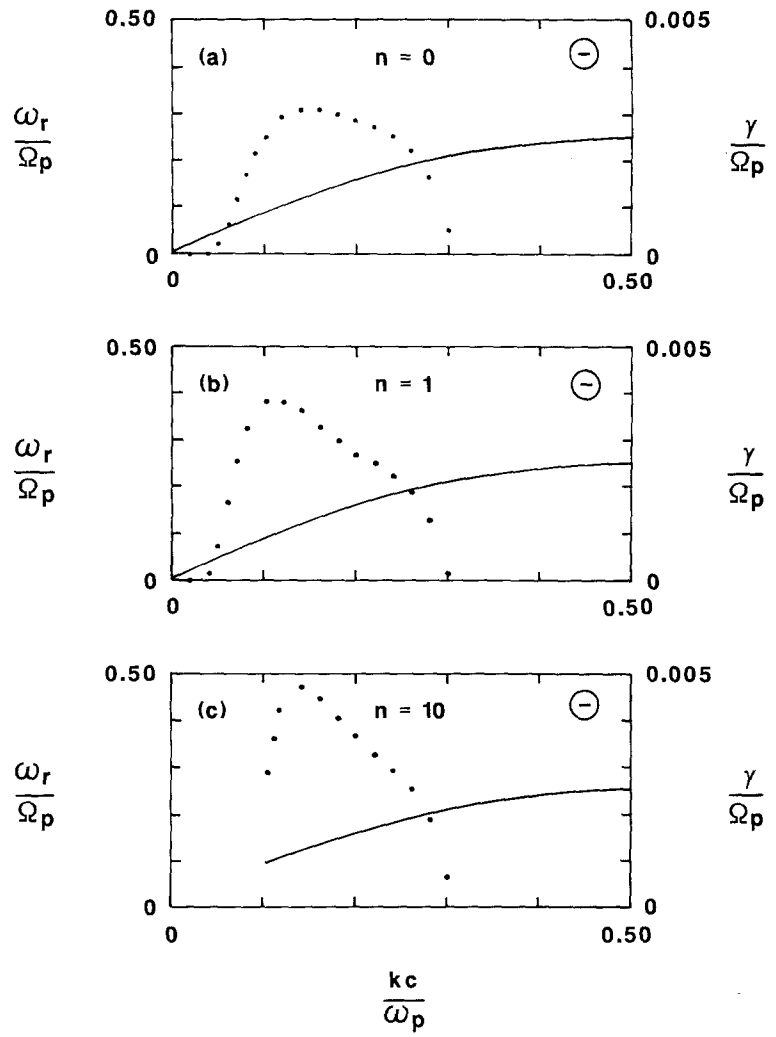

Fig. 9. The real frequency (solid lines) and growth rates (dotted lines) for the proton/proton left-hand resonant instability as a function of wave number. Parameters in panel (a) are those of Table I(b); parameters in panel (b) are those of Table I(e) with $n = 1$ and $T_s = 100T_c$ (thick shell); and parameters in panel (c) are those of Table I(e) with $n = 10$ and $T_s = 10T_c$ (thin shell). Here $\theta = 0°$.

Gary (1978a) showed that the primary role of the fluctuating fields of the right-hand resonant instability in the cool beam regime is not to take up momentum and energy lost by the beam, but rather to act as a medium by which the beam loses these quantities to the core component through pitch-angle scattering. Winske and Leroy (1984) used the Gary and Feldman (1978) formalism to show that beam energy loss for the right-hand resonant instability was much less important than dissipationless pitch-angle scattering, but also that deceleration, not pitch-angle scattering, was the dominant beam response to the ion/ion nonresonant instability. Winske and Leroy (1984) also compared their

second-order calculations with their computer simulations (see Section 6), and demonstrated qualitative, if not quantitative, agreement between results from the two approaches. Gary and Tokar (1985) applied the second-order theory at $\mathbf{k} \times \mathbf{B}_0 = 0$ to the complementary case of hot ion beams, in which the two important ion/ion instabilities are the right-hand and left-hand resonant modes. By combining the effects of both instabilities into a self-consistent quasilinear theory, Rogers *et al.* (1985) showed that a hot, tenuous ion beam somewhat above threshold leads to a roughly equal mixture of both polarizations while maintaining itself in a relatively isotropic condition.

The full velocity-space formalism for plasma interactions with electromagnetic instabilities was stated by Kennel and Engelmann (1966). Sagdeev *et al.* (1986) used such a theory to argue that heavy ions in the distant cometary environment could excite intense low frequency magnetic fluctuations and that scattering by these flucuations would lead to solar wind pickup of these ions. Lee and Ip (1987) applied such a theory to the problem of solar wind pickup of interstellar ions in which electromagnetic ion/ion instabilities provide the pickup mechanism. Their results indicate that pickup helium has an unobservable effect on the solar wind fluctuation spectrum, but that pickup hydrogen should produce substantial modifications near the cyclotron resonant frequency at sufficiently great distances from the Sun.

The conventional quasilinear theory of weak scattering by low-frequency electromagnetic fluctuations has an intrinsic problem: the pitch-angle scattering rate is proportional to the fluctuating magnetic field energy density at wave numbers in cyclotron resonance ($\omega_r - k_z v_z \pm m\Omega_j = 0$ with $m = 1, 2, \ldots$) with the particles. Since plasmas do not support modes of arbitrarily large wave number, there is no cyclotron resonance with particles at $v_z = 0$ and no scattering through pitch-angles perpendicular to $\mathbf{B}_0$. Thus, given a strongly anisotropic ion component such as a cool beam or ring-beam, conventional quasilinear theory cannot yield an isotropic distribution. Since many of the observations described in Section 2 imply and many of the simulations discussed in Section 6 demonstrate, that weak scattering by resonant fluctuations can indeed produce nearly isotropic ion distributions, a certain amount of apologetics are necessary whenever this theory is utilized to obtain such distributions. Although nonlinear processes such as resonance broadening (Lee and Ip, 1987) or trapping (Sagdeev *et al.*, 1986) are usually invoked to justify application of the formalism, weak temporal growth of the fluctuations can also provide a finite v_z width to the wave-particle resonance. The derivation of an appropriate diffusion coefficient that will resolve this difficulty is an outstanding unsolved problem.

Lee developed a quasilinear theory of electromagnetic ion/ion instabilities for the inhomogeneous plasma problem of first-order Fermi acceleration and applied it to both the Earth's bow shock (Lee, 1982) and to interplanetary shocks (Lee, 1983). The bow shock applications of this theory have been elaborated by Lee and Skadron (1985) and Skadron *et al.* (1988), and extended to the problem of ion Fermi acceleration at the Jovian bow shock by Smith and Lee (1986).

6. Computer Simulations

The major advantage of computer simulations over analytic theories is that, if they are properly done, simulations can include all appropriate nonlinear effects which contribute to the evolution of an instability. Thus a well-posed simulation will be without prejudice and will permit the physically most important nonlinear process to assert its dominance in a given situation. The major disadvantage of computer simulations is that it is often difficult to discern which nonlinear process is, in fact, asserting itself; this typically requires not only good diagnostics in the code, but an absence of prejudice on the part of the simulator as well as the simulation.

The first computer simulations of electromagnetic ion/ion instabilities for space applications were those of Winske and Leroy (1984), using a hybrid code described in Winske and Leroy (1985). In such a code the ions are represented as particles, whereas the electrons are described as a zero-mass, charge neutralizing fluid. Two-dimensional hybrid codes have been used by Winske and Quest (1986) and Thomas and Brecht (1988) to simulate both the ion/ion nonresonant and the right-hand resonant instabilities. Winske and Quest concluded that the 2-D code yields results in a homogeneous plasma that are qualitatively similar to those from the 1-D code, at least in the tenuous beam limit.

Ion/ion instabilities have also been simulated through the use of three other types of codes. Hoshino and Terasawa (1985) used a full particle code, in which both ions and electrons are treated as discrete particles; they demonstrated that electron kinetic effects are not of great importance in simulations of the ion/ion right-hand resonant instability. The codes of Hada *et al.* (1987) and Zachary *et al.* (1989) go to the opposite extreme and model both the electrons and one ion component as magnetized fluids. The advantage of using a fluid representation for one or more components is that the simulations need follow fewer particles and can, therefore, be run in larger systems and for longer times; the disadvantage is that the fluid approximation neglects kinetic physics such as wave-particle resonance effects. Unless noted otherwise, the results described in the remainder of this section are concerned with applications of one-dimensional hybrid computer codes similar to the code described by Winske and Leroy (1985).

Winske and Leroy (1984) simulated the cool beam case at several different proton beam densities, thereby obtaining growth of both the right-hand resonant and nonresonant instabilities. Their results clearly showed the exponential temporal growth of the instability, saturation of the fluctuating magnetic fields, and rapid pitch-angle scattering of the cool beam through intermediate-like, bean-shaped distributions to a broad, diffuse-like suprathermal component. They also demonstrated that at $v_A \ll v_0$ both the ion/ion nonresonant and right-hand resonant instabilities saturated at similar levels. Winske and Gary (1986) generalized this result to the case of heavy ion beams and argued that, when the free energy in the beam is fairly large, the saturation level for both instabilities can be estimated by assuming that roughly half of the beam energy ends

up in the fluctuations:

$$\frac{|\delta B|^2}{B_0^2} \simeq \frac{n_b}{2n_e}\,\frac{m_b}{m_p}\,\frac{v_{0b}^2}{v_A^2}\,, \quad n_b \ll n_e\,. \tag{23}$$

Winske *et al.* (1985) carried out hybrid simulations of the right-hand resonant instability driven by a heavy ($m_b = 6m_p$) cold ion ring-beam at $\alpha = 45°$; the results were quite similar to those of Winske and Leroy (1984) for the proton/proton right-hand resonant mode. Thomas and Brecht (1986) used a 2-D hybrid simulation to show that the right-hand resonant instability could also grow in a plasma slug of limited extent parallel to $\mathbf{B}_0$. Hoshino and Terasawa (1985) simulated the right-hand resonant instability with a full particle code, and showed that, as a cool ion beam interacts with a growing monochromatic magnetic fluctuation, it becomes 'gyrophase bunched'; that is, the beam becomes strongly non-gyrotropic and its average perpendicular velocity vector maintains a uniform phase angle with respect to the phase angle of the fluctuating magnetic field $\delta\mathbf{B}$.

In contrast, Gary *et al.* (1986b) showed that, at drift speeds not too far above threshold, the right-hand resonant instability saturated with a different scaling for the fluctuating field energy density:

$$\frac{|\delta B|^2}{B_0^2} \simeq \frac{n_b}{4n_e}\,\frac{v_{0b}^4}{v_A^4}\,, \qquad n_b \ll n_e \quad \text{and} \quad m_b = m_p\,. \tag{24}$$

Gary *et al.* (1986b) also showed that the ion beam response was quasilinear in this regime; that is, wave-particle scattering both reduced v_0/v_A and increased $T_{\perp b}/T_{\parallel b}$ so that saturation took place when the changes in these two parameters corresponded to zero growth in the linear dispersion equation.

Computer simulations to model the distant cometary environment have been carried out by Gary *et al.* (1986c, 1988, 1989). These simulations used the same Winske and Leroy (1985) code with one important difference: instead of a constant beam component density, the tenuous ion component is injected at a constant rate throughout the simulation in order to model the ionization of cometary neutrals. These self-consistent simulations, as well as those of Gaffey *et al.* (1988) and the test particle computations of Wu *et al.* (1986) and Price and Wu (1987), demonstrate that pitch-angle scattering by enhanced low-frequency electromagnetic waves leads to the formation of relatively complete velocity shell distributions similar to those observed in the distant environment of Comet Halley. Wu *et al.* (1986) and Gaffey *et al.* (1988) also have emphasized that the time for pitch-angle scattering to a relatively thin, relatively complete shell in velocity space is considerably faster than the energy scattering time for broadening of the shell toward a thermal distribution.

Since the cometary simulations of Gary *et al.* (1986c, 1988, 1989) were self-consistent, the authors were able to draw several conclusions about field, as well as plasma, properties. They found that the fluctuating field growth could be classified into one of two distinct regimes, which may be summarized as follows: at the relatively weak

free-energy injection rates of proton injection, the fluctuating field energy density at the relatively short wavelengths of the proton-cyclotron resonant exhibits lilnear temporal growth at early times, then gradually approaches an asymptotic, constant regime at late times. The equation characterizing linear temporal growth is, for an ion injection rate $(\mathrm{d}n_b/\mathrm{d}t)/n_c$ = constant,

$$\frac{\mathrm{d}}{\mathrm{d}t}\frac{\sum_k |\delta B_k|^2}{8\pi} = \sigma_b \frac{\mathrm{d}n_b}{\mathrm{d}t}\frac{m_b v_{0b}^2}{2}, \tag{25}$$

where σ_b is a constant. Gary *et al.* (1988, 1989) used a large number of simulations at $\mathbf{k} \times \mathbf{B}_0 = 0$ to infer that

$$\sigma_b(\alpha) \simeq \sigma_b(0)\left(\frac{2 + \cos 2\alpha}{3}\right),$$

where $\sigma_b(0) = 0.06 \pm 0.02$ at $v_0 \lesssim 10 v_A$. At the relatively strong free-energy injection rates corresponding to oxygen-ion injection, a single Fourier mode emerges from the noise to exhibit exponential temporal growth. This mode corresponds closely to the wave number of maximum growth of the long wavelength oxygen-ion/proton right-hand resonant instability as predicted by linear theory based on a beam of fixed density. Relatively quickly ($\Omega_p t \lesssim 1000$) magnetic trapping leads to a peak value of ε_{Bk} which scales as

$$\frac{|\delta B_k|^2}{B_0^2} \simeq 10\left(\frac{m_b}{m_c}\right)^2\left(\frac{v_{0b}}{v_A}\right)^2\frac{\Lambda_b}{\Omega_p}\cos^8\alpha, \quad (0° \leq \alpha \lesssim 45°). \tag{26}$$

Omidi and Winske (1986, 1987) also carried out simulations of the distant cometary environment, but considered larger scale configuration space issues associated with plasma inhomogeneities. By running simulations at both $\alpha = 5°$ and $90°$, they convincingly demonstrated that cometary ion pickup in quasi-perpendicular regions was due to the relatively rapid process of ion gyromotion, whereas low-frequency ion/ion instabilities led to pickup in quasi-parallel regions, albeit at a considerably slower rate.

Finally, the issue of nonlinear wave steepening to form shocklets has been studied by Hada *et al.* (1987) and by Omidi and Winske (1988, 1990). The former authors began with a large amplitude, almost linearly polarized wave and showed that wave steepening and wave packet formation occurred in their simulation. Omidi and Winske carried out a two-stage simulation; in the first stage the ion/ion right-hand resonant instability grew at propagation oblique to $\mathbf{B}_0$ in a large non-periodic box, while the much higher resolution of the second stage demonstrated further growth and evolution of an isolated fluctuation. These simulations exhibited the formation of both a long wavelength, linearly polarized shocklet, and an associated short wavelength, right-hand polarized whistler wave packet which strongly resemble the wave forms seen in both the terrestrial foreshock and near Comet Giacobini–Zinner.

7. Applications

7.1. Solar wind

There are at least two distinct models for the development of two proton component distributions in the solar wind. Livi and Marsch (1987) have developed a kinetic model in which the combined action of the expanding interplanetary magnetic field and decreasing collisional scattering causes ion distributions streaming outward in the solar wind to become strongly anisotropic and, under appropriate conditions, to develop a resolved double peak. In contrast, the conceptual model of Feldman *et al.* (1974) attributes double ion streams in the solar wind to fast plasma from the solar corona overtaking slower plasma emitted from the Sun at earlier times.

Although there have been extensive studies of two proton component distributions in the solar wind (e.g., Marsch and Livi, 1987), there has been little analysis addressing the critical issues necessary to determine which is the more appropriate model for generation of the two components. The Livi and Marsch (1987) model predicts that the two components should become better resolved as distance from the Sun increases, whereas the Feldman *et al.* (1974) model predicts the opposite consequence. Theory then predicts that this increased resolution should correspond to increased activity of the right-hand resonant instability, including stronger fluctuations at proton resonant frequencies and a $T_{\perp b}/T_{\parallel b}$ increasingly greater than unity. Such topics would be appropriate subjects for analysis of data not only from the Helios spacecraft (from which the Marsch *et al.* (1982) analysis seems to favor the Feldman *et al.* model), but also from the Ulysses spacecraft after its launch in 1990.

7.2. The terrestrial bow shock

The Earth's bow shock is apparently a source of cool beams of relatively energetic ions which stream along the magnetic field B_0 into the foreshock. Theory and computer simulations predict that such beams drive electromagnetic ion/ion instabilities with the right-hand resonant mode most likely to arise under typical foreshock conditions; Watanabe and Terasawa (1984) have used magnetic fluctuation observations to confirm this prediction.

Ion/ion instabilities lead to large amplitude, low-frequency magnetic fluctuations which, in turn, scatter the cool field-aligned beam. Interaction with a monochromatic resonant fluctuation leads to the development of a gyrophase-bunched beam; Fuselier *et al.* (1986a) showed that the observed beam-wave relative phases are in accord with theoretical predictions for the right-hand resonant instabiliity. A broader fluctuation wave spectrum aparently scatters the beam into the gyrotropic intermediate distributions; in either case, the final, strongly scattered state of the beam is the hot diffuse component. Gosling *et al.* (1989a) have recently reviewed competing models for the source of diffuse distributions in the terrestrial foreshock, and have exhibited two diffuse events which are very likely due to scattering by the co-existing magnetic fluctuations.

The simulations of Omidi and Winske (1988, 1990) have demonstrated that the

shocklets and whistler wave packets of the terrestrial foreshock and the Giacobini–Zinner environment result from the nonlinear evolution of the ion/ion right-hand resonant instability. Since the shocklet formation theory of Hada *et al.* (1987) requires wave refraction across a boundary separating plasmas with different wave properties, Le *et al.* (1989a) have argued that the absence of a distinct foreshock region at the comet favors a direct steepening model such as that of Omidi and Winske as the proper explanation for shocklet formation. A question which remains here is (N. Omidi, private communication): since the ion/ion right-hand resonant instabiliity grows most rapidly at $\mathbf{k} \times \mathbf{B}_0 = 0$, why do the slower growing compressible modes at oblique propagation, which is necessary to form shocklets, dominate the final nonlinear state? The simulations of Gary *et al.* (1988), in which the more slowly growing oxygen-ion/proton instability reaches a much larger amplitude than the faster growing proton/proton mode, may provide a clue here.

Another foreshock phenomenon which may be related to electromagnetic ion/ion instabilities is that of the 'hot diamagnetic cavities', rare, localized regions in which solar wind flow kinetic energy appears to have been converted to plasma thermal energy (Thomsen *et al.*, 1988; Paschmann *et al.*, 1988; Schwartz *et al.*, 1988). Thomsen *et al.* (1988) hypothesize that these structures may form from unusually strong interactions between shock-reflected ions and the solar wind, in which the wave-particle interaction is due to the ion/ion nonresonant instability. The two-dimensional hybrid simulations of Thomas and Brecht (1988) support this hypothesis by showing that an ion beam of finite extent can indeed yield growing fluctuations which produce an energetic plasma which, in turn, pushes away the ambient magnetic field. One discrepancy here is that Thomas and Brecht appear to see the right-hand resonant instability, rather than the nonresonant growing mode.

The computer simulations of Quest *et al.* (1983) have demonstrated that ions reflected from a quasi-parallel shock can form an upstream ring-beam component. But the enhanced magnetic fluctuations in this and other early simulations of quasi-parallel shocks (Kan and Swift, 1983) are relatively high-frequency whistler-like, so the role of ion/ion instabilities in the physics is not clear. More recently, Quest (1988) has used hybrid simulations to develop a comprehensive theory of parallel shocks in which shock formation and plasma heating result from electromagnetic ion/ion instabilities associated with the counterstreaming of upstream and downstream plasmas. In the Quest model, the ion/ion nonresonant instability contributes to shock formation and during transient periods, whereas under late time, steady-state conditions, the right-hand resonant instability determines the foreshock structure and shock dissipation. Recently there has been an increase in interest in quasi-parallel shocks; ongoing observational as well as computational studies are currently addressing questions such as the applicability of the Quest model to quasi-parallel shocks and the role of reflected ions and the associated ion/ion instabilities.

7.3. Other shocks

Probably the most interesting recent application of ion/ion instability theory to interplanetary shocks has been the work of Kennel *et al.* (1986), who compared ISEE-3 observations of the 12 November, 1978 interplanetary shock against thirteen predictions of Lee's (1983) quasilinear theory of Fermi acceleration. Kennel *et al.* (1986) concluded that the theory accounted, with varying degrees of precision, for almost all of the observations, thereby providing one of the rare examples in space plasma physics in which theory has led experiment.

Initial studies of the large-amplitude, low-frequency magnetic fluctuations at the Jovian bow shock concluded that they were right-hand polarized in the solar wind frame. This led to the interpretation that they, like the fluctuations in the terrestrial foreshock, are due to the ion/ion right-hand resonant instability (Smith *et al.*, 1983; Goldstein *et al.*, 1983). Later examination of the fluctuation data yielded a left-hand polarization; the resulting reinterpretation then associated their source to be either relativistic electrons (Smith *et al.*, 1976; Goldstein *et al.*, 1985) or hot heavy ions (Goldstein *et al.*, 1986) streaming away from the Jovian bow shock.

In Saturn's foreshock Behannon *et al.* (1985) observed enhanced magnetic fluctuations that are, like those observed in the terrestrial foreshock, primarily right-hand polarized in the plasma frame. These authors expressed concern that the fluctuations are one to two orders of magnitude lower frequency than terrestrial or Jovian foreshock waves. However, the fluctuations at Saturn are not strongly Doppler shifted and correspond to plasma frame frequencies $0.01 \lesssim \omega_r/\Omega_p \lesssim 0.05$, which is only a factor of two less than the plasma frame frequencies of fluctuations in Earth's foreshock (Hoppe and Russell, 1983; Watanabe and Terasawa, 1984). Thus, as Behannon *et al.* (1985) concluded, these fluctuations are similar to their terrestrial counterparts. Further significant progress in understanding low-frequency fluctuations near non-terrestrial planets will require more data, especially with respect to the suprathermal ions, which we hope will be provided by the Galileo and Cassini probes of the next decade.

7.4. The plasma sheet boundary layer

Although thermal or suprathermal ions were not measured during the ISEE-3 passes through the distant plasma sheet boundary layer, Tsurutani *et al.* (1985) identified the $\omega_r \sim \Omega_p$ fluctuations observed there as due to the ion/ion right-hand resonant instability. Gary *et al.* (1986b) argued that their simulations in the quasilinear regime should be a model for the nonlinear response of ion beams in this region, and, as a consequence, they predicted that these beams should be relatively anisotropic ($T_{\perp b} > T_{\parallel b}$) and relatively dense ($n_b \simeq 0.10 n_e$).

Ion observations in the plasma sheet boundary layer closer to Earth are not dissimilar to the Gary *et al.* (1986b) predictions: the single streaming or double counterstreaming ion beams are relatively dense ($n_b \lesssim 0.5 n_e$) and often strongly anisotropic ($T_{\parallel b} \ll T_{\perp b}$) (Takahashi and Hones, 1988, and references therein). In the near-Earth plasma sheet boundary layer, Angelopoulos *et al.* (1989) examined the linear stability of such distribu-

tions observed during two ISEE crossings of this region. Unlike conditions thought to obtain in the deep tail, $v_0 \lesssim v_A$ in the near-Earth boundary layer, and electromagnetic ion/ion instabilities are not excited. However, because $T_\perp \gg T_\parallel$ for these ion components, both parallel and antiparallel propagating branches of the ion-cyclotron anisotropy instability may arise. In particular, Angelopoulos *et al.* (1989) have shown that, when the anisotropy of one counterstreaming component is sufficiently large and lies on the ion component of greater density, the Doppler shifted frequency of one branch of the ion-cyclotron anisotropy instability in the spacecraft frame lies well above Ω_p. Magnetic data do, in fact, exhibit enhanced fluctuations at such frequencies, providing confirmation of the theoretical interpretation. Further theoretical research on boundary layer topics should address nonlinear questions: Since the distributions appear to be strongly unstable, why are the observed fluctuation levels so weak? In spite of the low fluctuation amplitudes, is wave-particle scattering of the streaming ions important, and can it contribute to thermalization of the plasma sheet?

7.5. Cometary environments

Cometary ion distribution functions well beyond the Halley bow shock have been observed as broadened ring-beams or partial shells in velocity space (Coates *et al.*, 1989; Neugebauer *et al.*, 1989). At $\alpha \lesssim 60°$, such distributions are most likely to drive the right-hand resonant instability (Winske *et al.*, 1985a), which approximately satisfies the $m = 1$ cyclotron resonance condition, Equation (16) (e.g., Figure 1 of Gary *et al.*, 1989). As pointed out by Tsurutani and Smith (1986b), instabilities which are driven by newborn cometary ions and which satisfy this condition in the solar wind frame of reference should appear as fluctuations at the corresponding ion-cyclotron frequency in the spacecraft frame. This fortuitous elimination of the Doppler shift has permitted a clear experimental delineation between the proton/proton and water-group-ion/proton right-hand resonant instabilities, and has facilitated progress in the identification of fluctuation properties in the distant cometary environment. In quasi-parallel regimes such that $\alpha \lesssim 60°$, fluctuations near the water-group-ion cyclotron frequency have been identified as due to the ion/ion right-hand resonant instability (Tsurutani *et al.*, 1987a, 1989a; Glassmeier *et al.*, 1989), as was predicted by Winske and Gary (1986). In quasi-perpendicular regimes ($70° \lesssim \alpha \leq 90°$) cometary ion instabilities no longer satisfy Equation (16) and mode identification is more difficult, although Glassmeier *et al.* (1989) report some evidence of left-hand polarization, commensurate with the prediction of Gary and Schriver (1987).

Fluctuation observations in the distant cometary environment which have been modeled by the simulations of Gary *et al.* (1988, 1989) include: (i) Magnetic fluctuation spectra at relatively small α have distinct peaks near the water-group-ion cyclotron resonant wave number (Tsurutani and Smith, 1986a; Glassmeier *et al.*, 1989). (ii) Large amplitude magnetic fluctuations observed near the water-group ion cyclotron frequency at $\alpha \lesssim 60°$ are no longer observed by Tsurutani *et al.* (1989a) when α increases to $70°$–$90°$. (iii) Magnetic fluctuation spectra near the proton-cyclotron resonant wave number at all α values have no clearly resolved peak (Tsurutani and Smith, 1986a;

Tsurutani *et al.*, 1989b; Glassmeier *et al.*, 1989); and (iv) There is a linear correlation between the cometary proton energy density and the fluctuating field energy density (Neugebauer and Neubauer, 1988). And there have been two model predictions of fluctuating magnemtic field amplitudes which show agreement with observations as a function of cometocentric distance. Galeev *et al.* (1986) computed $|\delta B|^2$ by balancing instability growth due to the anisotropy of the cometary ions with wave energy transfer to longer wavelengths due to induced scattering of waves by solar wind protons; their results showed good agreement with magnetic field energy densities in the water-group-ion cyclotron frequency range observed by the Vega spacecraft at Halley. The Gary *et al.* scalings for $|\delta B|^2$ (Equation (25) and Equation (26)) have also been converted to functions of cometocentric distance, with good agreement with the Giacobini–Zinner ICE observations at both the proton cyclotron (Le *et al.*, 1989b) and the water-group ion cyclotron (Figure 9(a) of Gary *et al.*, 1988) frequencies.

In spite of the many recent studies of electromagnetic ion/ion instabilities in the cometary environment, several questions on this topic remain. How much of the partial shell broadening observed by Coates *et al.* (1989) and Neugebauer *et al.* (1989) is due to stochastic pitch-angle scattering by resonant magnetic fluctuations, and how much is due to ionization at different α values due to the presence of very low-frequency, large amplitude ambient waves in the solar wind? Do electromagnetic ion/ion instabilities contribute to the rapid thermalization of both the cometary ions and solar wind ions observed at the Halley bow shock (Wilken *et al.*, 1987; Neugebauer *et al.*, 1987b; Verigin *et al.*, 1987)? What is the relative importance of first-order and second-order Fermi acceleration processes in the cometary environment (Ip and Axford, 1986; Gribov *et al.*, 1987; Isenberg, 1987; Gombosi, 1988), and what roles do ion/ion instabilities play in these two processes?

Acknowledgements

The author acknowledges the contributions of each of the co-authors of the Gary *et al.* papers cited in this review. He also acknowledges useful discussions with Jack Gosling, Martin Lee, Nick Omidi, and Michelle Thomsen, helpful comments on the manuscript by Armando Brinca and Bruce Tsurutani, as well as Dan Winske's support in the use of the hybrid simulation code. This work was performed under the auspices of the U.S. Department of Energy, and was supported by the DOE Office of Basic Energy Sciences, Geosciences, and the National Aeronautics and Space Administration.

Appendix

We consider a steady, uniform background magnetic field $\mathbf{B}_0 = \hat{\mathbf{z}} B_0$, and derive the fully electromagnetic dispersion equation for plasma instabilities associated with Maxwellian distribution functions with drift velocities parallel to $\mathbf{B}_0$.

For propagation at arbitrary angles with respect to $\mathbf{B}_0$ it is convenient to define the

dimensionless conductivity tensor of the jth component $\mathbf{S}_j(\mathbf{k}, \omega)$:

$$\mathbf{\Gamma}_j^{(1)}(\mathbf{k}, \omega) = -\frac{ik^2c^2}{4\pi e_j \omega}\, \mathbf{S}_j(\mathbf{k}, \omega) \cdot \mathbf{E}^{(1)}(\mathbf{k}, \omega)\,. \tag{A.1}$$

If we combine Equation (A.1) with Faraday's equation and the Ampère/Maxwell equation we obtain

$$\mathbf{D} \cdot \mathbf{E}^{(1)} = 0\,, \tag{A.2}$$

where, with $\mathbf{k} = \hat{\mathbf{y}} k_y + \hat{\mathbf{z}} k_z$,

$$\begin{aligned}
D_{xx} &= \omega^2 - k^2c^2 + k^2c^2 \sum_j S_{xxj}\,,\\
D_{xy} &= k^2c^2 \sum_j S_{xyj}\,,\\
D_{xz} &= k^2c^2 \sum_j S_{xzj}\,,\\
D_{yx} &= k^2c^2 \sum_j S_{yxj}\,,\\
D_{yy} &= \omega^2 - k_z^2c^2 + k^2c^2 \sum_j S_{yyj}\,,\\
D_{yz} &= k_y k_z c^2 + k^2c^2 \sum_j S_{yzj}\,,\\
D_{zx} &= k^2c^2 \sum_j S_{zxj}\,,\\
D_{zy} &= k_y k_z c^2 + k^2c^2 \sum_j S_{zyj}\,,\\
D_{zz} &= \omega^2 - k_y^2c^2 + k^2c^2 \sum_j S_{zzj}\,.
\end{aligned} \tag{A.3}$$

The dispersion equation for the various plasma modes of the system is then

$$\det|\mathbf{D}| = 0\,. \tag{A.4}$$

From Equation (A.2) we may obtain the relative values of the fluctuating field components. In particular,

$$\frac{E_z^{(1)}}{E_y^{(1)}} = \frac{D_{xx}D_{zy} - D_{zx}D_{xy}}{D_{zx}D_{xz} - D_{xx}D_{zz}} \tag{A.5z}$$

and

$$\frac{E_x^{(1)}}{E_y^{(1)}} = \frac{D_{zz}D_{xy} - D_{xz}D_{zy}}{D_{zx}D_{xz} - D_{xx}D_{zz}}\,. \tag{A.5x}$$

To evaluate $\mathbf{S}_j(\mathbf{k}, \omega)$, we use the linear Vlasov equation for electromagnetic waves in

a magnetized plasma:

$$\frac{\partial f_j^{(1)}(\mathbf{x}, \mathbf{v}, t)}{\partial t} + \mathbf{v} \cdot \frac{\partial f_j^{(1)}}{\partial \mathbf{x}} + \frac{e_j}{m_j}\left(\frac{\mathbf{v} \times \mathbf{B}_0}{c}\right) \cdot \frac{\partial f_j^{(1)}}{\partial \mathbf{v}} =$$

$$= -\frac{e_j}{m_j}\left[\mathbf{E}^{(1)}(\mathbf{x}, t) + \frac{\mathbf{v} \times \mathbf{B}^{(1)}(\mathbf{x}, t)}{c}\right] \cdot \frac{\partial f_j^{(0)}(\mathbf{v})}{\partial \mathbf{v}} . \qquad \text{(A.6)}$$

From the linear Vlasov Equation (A.6) and Faraday's equation the first-order distribution function of the jth component may be written in terms of an integration over unperturbed orbits:

$$f_j^{(1)}(\mathbf{k}, \mathbf{v}, \omega) = -\frac{e_j}{m_j} \int_{-\infty}^{0} d\tau \left[\frac{\partial f_j^{(0)}}{\partial \mathbf{v}'} + \frac{\mathbf{k}}{\omega} \times \left(\mathbf{v}' \times \frac{\partial f_j^{(0)}}{\partial \mathbf{v}'}\right)\right] \cdot \mathbf{E}^{(1)}(\mathbf{k}, \omega) \times$$

$$\times \exp[ib_j(\tau, \omega)] , \qquad \text{(A.7)}$$

where $\tau = t' - t$, a prime indicates an unperturbed orbit variable and

$$b_j(\tau, \omega) \equiv \frac{k_y v_x}{\Omega_j} (\cos \Omega_j \tau - 1) + \frac{k_y v_y}{\Omega_j} \sin \Omega_j \tau + (k_z v_z - \omega)\tau .$$

Using the zeroth-order drifting Maxwellian distribution function (10),

$$f_j^{(1)}(\mathbf{k}, \mathbf{v}, \omega) = \frac{e_j}{T_j} f_j^{(M)}(\mathbf{v} - \mathbf{v}_{0j})\left(1 - \frac{\mathbf{k} \cdot \mathbf{v}_{0j}}{\omega}\right) \int_{-\infty}^{0} d\tau \mathbf{v}' \cdot \mathbf{E}^{(1)}(\mathbf{k}, \omega) \times$$

$$\times \exp[ib_j(\tau, \omega)] - \frac{e_j}{T_j} f_j^{(M)}(\mathbf{v} - \mathbf{v}_{0j}) \mathbf{v}_{0j} \cdot \mathbf{E}^{(1)}(\mathbf{k}, \omega) \times$$

$$\times \int_{-\infty}^{0} d\tau \left(1 - \frac{\mathbf{k} \cdot \mathbf{v}'}{\omega}\right) \exp[ib_j(\tau, \omega)] .$$

The dimensionless conductivity tensor is then, using Equation (A.1),

$$\mathbf{S}_j(\mathbf{k}, \omega) =$$

$$= \frac{ik_j^2}{k^2 n_j c^2} (\omega - \mathbf{k} \cdot \mathbf{v}_{0j}) \int d^3v (\mathbf{v} + \mathbf{v}_{0j}) f_j^{(M)}(\mathbf{v}) \int_{-\infty}^{0} d\tau (\mathbf{v}' + \mathbf{v}_{0j}) \times$$

$$\times \exp[ib_j(\tau, \omega - \mathbf{k} \cdot \mathbf{v}_{0j})] + \frac{k_j^2}{k^2} \frac{\mathbf{v}_{0j} \mathbf{v}_{0j}}{c^2} . \qquad \text{(A.8)}$$

Thus

$$\mathbf{S}_j(\mathbf{k}, \omega) = \mathbf{S}_j^{(M)}(\mathbf{k}, \omega - \mathbf{k}\cdot\mathbf{v}_{0j}) + \frac{\mathbf{v}_{0j}}{c}\,\mathbf{Q}_j^{(M)}(\mathbf{k}, \omega - \mathbf{k}\cdot\mathbf{v}_{0j}) +$$

$$+ \mathbf{R}_j^{(M)}(\mathbf{k}, \omega - \mathbf{k}\cdot\mathbf{v}_{0j})\,\frac{\mathbf{v}_{0j}}{c} + \frac{\mathbf{v}_{0j}\mathbf{v}_{0j}}{c^2}\,K_j^{(M)}(\mathbf{k}, \omega - \mathbf{k}\cdot\mathbf{v}_{0j})\,, \quad \text{(A.9)}$$

where the superscript (M) denotes quantities derived from the Maxwellian distribution function:

$$\mathbf{S}_j^{(M)}(\mathbf{k}, \omega) = \frac{ik_j^2\omega}{k^2 n_j c^2}\int \mathrm{d}^3v\,\mathbf{v} f_j^{(M)}(\mathbf{v}) \int_{-\infty}^{0} \mathrm{d}\tau\,\mathbf{v}'\,\exp[ib_j(\tau, \omega)]\,,$$

$$\mathbf{Q}_j^{(M)}(\mathbf{k}, \omega) = \frac{ik_j^2\omega}{k^2 c n_j}\int \mathrm{d}^3v\, f_j^{(M)}(\mathbf{v}) \int_{-\infty}^{0} \mathrm{d}\tau\,\mathbf{v}'\,\exp[ib_j(\tau, \omega)]\,,$$

$$\mathbf{R}_j^{(M)}(\mathbf{k}, \omega) = \frac{ik_j^2\omega}{k^2 c n_j}\int \mathrm{d}^3v\,\mathbf{v} f_j^{(M)}(\mathbf{v}) \int_{-\infty}^{0} \mathrm{d}\tau\,\exp[ib_j(\tau, \omega)]\,,$$

and

$$K_j^{(M)}(\mathbf{k}, \omega) = \frac{k_j^2}{k^2}\left\{1 + \frac{i\omega}{n_j}\int \mathrm{d}^3v\, f_j^{(M)}(\mathbf{v}) \int_{-\infty}^{0} \mathrm{d}\tau\,\exp[ib_j(\tau, \omega)]\right\}.$$

Evaluating these quantities in the traditional manner, we obtain

$$S_{xxj}^{(M)}(\mathbf{k}, \omega) = \frac{\omega_j^2}{k^2c^2}\,\zeta_j^0\exp(-\lambda_j)\sum_{m=-\infty}^{\infty}\left\{2\lambda_j[I_m(\lambda_j) - I_m'(\lambda_j)] + \right.$$

$$\left. + \frac{m^2}{\lambda_j}\,I_m(\lambda_j)\right\} Z(\zeta_j^m)\,,$$

$$S_{xyj}^{(M)}(\mathbf{k}, \omega) = i\,\frac{\omega_j^2}{k^2c^2}\,\zeta_j^0\exp(-\lambda_j)\sum_{m=-\infty}^{\infty} m[I_m(\lambda_j) - I_m'(\lambda_j)]Z(\zeta_j^m)\,,$$

$$S_{xzj}^{(M)}(\mathbf{k}, \omega) = i\,\frac{\omega_j^2}{k^2c^2}\,\frac{|k_z|}{\sqrt{2}\,k_z}\,\zeta_j^0\,\frac{k_y v_j}{\Omega_j}\times$$

$$\times\exp(-\lambda_j)\sum_{m=-\infty}^{\infty}[I_m(\lambda_j) - I_m'(\lambda_j)]Z'(\zeta_j^m)\,,$$

$$S_{yxj}^{(M)}(\mathbf{k}, \omega) = -S_{xyj}^{(M)}(\mathbf{k}, \omega),$$

$$S_{yyj}^{(M)}(\mathbf{k}, \omega) = \frac{\omega_j^2}{k^2 c^2} \zeta_j^0 \frac{\exp(-\lambda_j)}{\lambda_j} \sum_{m=-\infty}^{\infty} m^2 I_m(\lambda_j) Z(\zeta_j^m),$$

$$S_{yzj}^{(M)}(\mathbf{k}, \omega) = \frac{\omega_j^2}{k^2 c^2} \frac{|k_z|}{\sqrt{2}\, k_z} \zeta_j^0 \frac{\Omega_j}{k_y v_j} \exp(-\lambda_j) \sum_{m=-\infty}^{\infty} m I_m(\lambda_j) Z'(\zeta_j^m),$$

$$S_{zxj}^{(M)}(\mathbf{k}, \omega) = -S_{xzj}^{(M)}(\mathbf{k}, \omega),$$

$$S_{zyj}^{(M)}(\mathbf{k}, \omega) = S_{yzj}^{(M)}(\mathbf{k}, \omega),$$

$$S_{zzj}^{(M)}(\mathbf{k}, \omega) = -\frac{\omega_j^2}{k^2 c^2} \zeta_j^0 \exp(-\lambda_j) \sum_{m=-\infty}^{\infty} I_m(\lambda_j) \zeta_j^m Z'(\zeta_j^m),$$

$$\mathbf{Q}_j^{(M)}(\mathbf{k}, \omega) = \frac{k_j^2}{k^2} \frac{v_j}{c} \zeta_j^0 \left\{ i\hat{\mathbf{x}} \frac{k_y v_j}{\Omega_j} \exp(-\lambda_j) \sum_m [I_m(\lambda_j) - I_m'(\lambda_j)] Z(\zeta_j^m) - \right.$$

$$- \hat{\mathbf{y}} \frac{\Omega_j}{k_y v_j} \exp(-\lambda_j) \sum_m m I_m(\lambda_j) Z(\zeta_j^m) -$$

$$\left. - \hat{\mathbf{z}} \frac{|k_z|}{\sqrt{2}\, k_z} \exp(-\lambda_j) \sum_m I_m(\lambda_j) Z'(\zeta_j^m) \right\},$$

$$R_{xj}^{(M)}(\mathbf{k}, \omega) = -Q_{xj}^{(M)}(\mathbf{k}, \omega),$$

$$R_{yj}^{(M)}(\mathbf{k}, \omega) = Q_{yj}^{(M)}(\mathbf{k}, \omega),$$

$$R_{zj}^{(M)}(\mathbf{k}, \omega) = Q_{zj}^{(M)}(\mathbf{k}, \omega),$$

and

$$K_j^{(M)}(\mathbf{k}, \omega) = \frac{k_j^2}{k^2} \left[1 + \zeta_j^0 \exp(-\lambda_j) \sum_m I_m(\lambda_j) Z(\zeta_j^m) \right],$$

where $\lambda_j \equiv (k_y a_j)^2$ and $\zeta_j^m \equiv (\omega + m\Omega_j)/\sqrt{2}\,|k_z|\, v_j$. The linear dispersion code 'EVO' solves Equation (A.3) using the above conductivity elements without approximation and provides the numerical results reported in this paper.

At $\mathbf{k} \times \mathbf{B}_0 = 0$, there is $k_y = 0$. Writing $k = |k_z|$, the above expressions reduce to

$$S_{xxj}^{(M)}(\mathbf{k}, \omega) = \frac{1}{2} \frac{\omega_j^2}{k^2 c^2} \zeta_j^0 [Z(\zeta_j^{+1}) + Z(\zeta_j^{-1})],$$

$$S_{xyj}^{(M)}(\mathbf{k}, \omega) = -\frac{i}{2} \frac{\omega_j^2}{k^2 c^2} \zeta_j^0 [Z(\zeta_j^{+1}) - Z(\zeta_j^{-1})],$$

$$S_{xzj}^{(M)}(\mathbf{k}, \omega) = 0,$$

$$S^{(M)}_{yxj}(\mathbf{k}, \omega) = -S^{(M)}_{xyj}(\mathbf{k}, \omega),$$

$$S^{(M)}_{yyj}(\mathbf{k}, \omega) = S^{(M)}_{xxj}(\mathbf{k}, \omega),$$

$$S^{(M)}_{yzj}(\mathbf{k}, \omega) = 0,$$

$$S^{(M)}_{zxj}(\mathbf{k}, \omega) = 0,$$

$$S^{(M)}_{zyj}(\mathbf{k}, \omega) = 0,$$

$$S^{(M)}_{zzj}(\mathbf{k}, \omega) = -\frac{k_j^2}{k^2}\frac{v_j^2}{c^2}(\zeta_j^0)^2 Z'(\zeta_j^0),$$

$$R^{(M)}_{xj}(\mathbf{k}, \omega) = -Q^{(M)}_{xj}(\mathbf{k}, \omega) = 0,$$

$$R^{(M)}_{yj}(\mathbf{k}, \omega) = Q^{(M)}_{yj}(\mathbf{k}, \omega) = 0,$$

$$R^{(M)}_{zj}(\mathbf{k}, \omega) = Q^{(M)}_{zj}(\mathbf{k}, \omega) = -\frac{k_j^2}{k^2}\frac{v_j}{c}\frac{\omega}{2k_z v_j} Z'(\zeta_j^0),$$

$$K^{(M)}_{j}(\mathbf{k}, \omega) = -\frac{k_j^2}{2k^2} Z'(\zeta_j^0).$$

Thus, at $\mathbf{k} \times \mathbf{B}_0 = 0$, Equation (A.2) factors into two parts. For electrostatic modes with $E_z^{(1)} \neq 0$,

$$D_{zz} = \omega^2\left[1 - \sum_j \frac{k_j^2}{2k_z^2} Z'\left(\frac{\omega - \mathbf{k}\cdot\mathbf{v}_{0j}}{\sqrt{2}\,|k_z|\,v_j}\right)\right] = 0,$$

which, at $\omega^2 \neq 0$, yields the electrostatic dispersion equation for drifting Maxwellian distributions at $k_y = 0$.

In addition, transverse modes with $\mathbf{E}^{(1)}$ and $\mathbf{B}^{(1)}$ perpendicular to $\mathbf{B}_0$ may also propagate along the magnetic field. From the remainder of the dispersion equation one obtains

$$\begin{pmatrix} D_{xx} & D_{xy} \\ D_{yx} & D_{yy} \end{pmatrix}\begin{pmatrix} E_x^{(1)} \\ E_y^{(1)} \end{pmatrix} = 0, \tag{A.10}$$

from which follows the electromagnetic dispersion equation for $\mathbf{k} \times \mathbf{B}_0 = 0$:

$$\omega^2 - k^2c^2 + k^2c^2 \sum_j S_j^{\pm}(\mathbf{k}, \omega) = 0, \tag{A.11}$$

where

$$S_j^{\pm}(\mathbf{k}, \omega) = \frac{\omega_j^2}{k^2c^2}\zeta_j Z(\zeta_j^{\pm}) \tag{A.12}$$

and ζ_j and $\zeta_j^{\pm}$ are given by Equation (13).

References

Abraham-Shrauner, B., Asbridge, J. R., Bame, S. J., and Feldman, W. C.: 1979, *J. Geophys. Res.* **84**, 553.

Akimoto, K., Gary, S. P., and Omidi, N.: 1987, *J. Geophys. Res.* **92**, 11209.

Angelopoulos, V., Elphic, R. C., Gary, S. P., and Huang, C. Y.: 1989, *J. Geophys. Res.* **94**, 15373.

Barnes, A.: 1966, *Phys. Fluids* **9**, 1483.

Barnes, A.: 1970, *Cosmic Electrodyn.* **1**, 90.

Bame, S. J., Asbridge, J. R., Feldman, W. C., Gary, S. P., and Montgomery, M. C.: 1975, *Geophys. Res. Letters* **2**, 373.

Bame, S., Anderson, R. C., Asbridge, J. R., Baker, D. N., Feldman, W. C., Fuselier, S. A., Gosling, J. T., McComas, D. J., Thomsen, M. F., Young, D. T., and Zwickl, R. D.: 1986, *Science* **232**, 356.

Bavassano-Cattaneo, M. B., Moreno, G., Scotto, M. T., and Acuna, M.: 1987, *J. Geophys. Res.* **92**, 12413.

Behannon, K. W., Goldstein, M. L., Lepping, R. P., Wong, H. K., Mauk, B. H., and Krimigis, S. M.: 1985, *J. Geophys. Res.* **90**, 10791.

Bonifazi, C. and Moreno, G.: 1981, *J. Geophys. Res.* **86**, 4397.

Brinca, A. L. and Tsurutani, B. T.: 1987a, *Geophys. Res. Letters* **14**, 495.

Brinca, A. L. and Tsurutani, B. T.: 1987b, *Astron. Astrophys.* **187**, 311.

Brinca, A. L. and Tsurutani, B. T.: 1988, *J. Geophys. Res.* **93**, 48.

Brinca, A. L. and Tsurutani, B. T.: 1989a, *J. Geophys. Res.* **94**, 3.

Brinca, A. L. and Tsurutani, B. T.: 1989b, *J. Geophys. Res.* **94**, 5467.

Coates, A. J., Johnstone, A. D., Wilken, B., Jockers, K., and Glassmeier, K.-H.: 1989, *J. Geophys. Res.* **94**, 9983.

Cuperman, S.: 1981, *Rev. Geophys.* **19**, 307.

Davidson, R. C. and Ogden, J. M.: 1975, *Phys. Fluids* **18**, 1045.

DeCoster, R. J. and Frank, L. A.: 1979, *J. Geophys. Res.* **84**, 5099.

Dum, C. T., Marsch, E., and Pilipp, W.: 1980, *J. Plasma Phys.* **23**, 91.

Eastman, T. E., Frank, L. A., Peterson, W. K., and Lennartsson, W.: 1984, *J. Geophys. Res.* **89**, 1553.

Fairfield, D. H.: 1969, *J. Geophys. Res.* **74**, 3541.

Fairfield, D. H. and Behannon, K. W.: 1976, *J. Geophys. Res.* **81**, 3897.

Feldman, W. C., Asbridge, J. R., Bame, S. J., and Montgomery, M. D.: 1973, *J. Geophys. Res.* **78**, 2017.

Feldman, W. C., Asbridge, J. R., Bame, S. J., and Montgomery, M. D.: 1974, *Rev. Geophys.* **12**, 715.

Feldman, W. C., Baker, D. N., Bame, S. J., Birn, J., Gosling, J. T., Hones, E. W., Jr., and Schwartz, S. J.: 1985, *J. Geophys. Res.* **90**, 233.

Forbes, T. G., Hones, E. W., Bame, S. J., Asbridge, J. R., Paschmann, G., Sckopke, N., and Russell, C. T.: 1981, *Geophys. Res. Letters* **8**, 261.

Freund, H. P. and Wu, C. S.: 1988, *J. Geophys. Res.* **93**, 14277.

Fuselier, S. A., Thomsen, M. F., Gary, S. P., Bame, S. J., Russell, C. T., and Parks, G. K.: 1986a, *Geophys. Res. Letters* **13**, 60.

Fuselier, S. A., Thomsen, M. F., Gosling, J. T., Bame, S. J., and Russell, C. T.: 1986b, *J. Geophys. Res.* **91**, 91.

Gaffey, J. D., Jr., Winske, D., and Wu, C. S.: 1988, *J. Geophys. Res.* **93**, 5470.

Galeev, A. A., Gribov, B. E., Gombosi, T., Gringauz, K. I., Klimov, S. I., Oberz, P., Remizov, A. P., Riedler, W., Sagdeev, R. Z., Savin, S. P., Sokolov, A. Yu., Shapiro, V. D., Shevchenko, V. I., Szego, K., Verigin, M. I., and Yeroshenko, Ye. G.: 1986, *Geophys. Res. Letters* **13**, 841.

Gary, S. P.: 1978a, *Nucl. Fusion* **18**, 327.

Gary, S. P., 1978b, *J. Geophys. Res.* **83**, 2504.

Gary, S. P., 1985, *Astrophys. J.* **288**, 342.

Gary, S. P., 1986, *J. Plasma Phys.* **35**, 431.

Gary, S. P. and Feldman, W. C.: 1978, *Phys. Fluids* **21**, 72.

Gary, S. P. and Madland, C. D.: 1988, *J. Geophys. Res.* **93**, 235.

Gary, S. P. and Schriver, D.: 1987, *Planetary Space Sci.* **35**, 51.

Gary, S. P. and Sinha, R.: 1989, *J. Geophys. Res.* **94**, 9131.

Gary, S. P. and Tokar, R. L.: 1985, *J. Geophys. Res.* **90**, 65.

Gary, S. P. and Winske, D.: 1986, *J. Geophys. Res.* **91**, 13699.

Gary, S. P., Gosling, J. T., and Forslund, D. W.: 1981, *J. Geophys. Res.* **86**, 6691; Correction, 1984, *J. Geophys. Res.* **89**, 404.

Gary, S. P., Smith, C. W., Lee, M. A., Goldstein, M. L., and Forslund, D. W.: 1984, *Phys. Fluids* **27**, 1852; Correction, 1985, *Phys. Fluids* **28**, 438.
Gary, S. P., Madland, C. D., and Tsurutani, B. T.: 1985, *Phys. Fluids* **28**, 3691.
Gary, S. P., Thomsen, M. F., and Fuselier, S. A.: 1986a, *Phys. Fluids* **29**, 531.
Gary, S. P., Madland, C. D., Schriver, D., and Winske, D.: 1986b, *J. Geophys. Res.* **91**, 4188.
Gary, S. P., Hinata, S., Madland, C. D., and Winske, D.: 1986c, *Geophys. Res. Letters* **13**, 1364.
Gary, S. P., Madland, C. D., Omidi, N., and Winske, D.: 1988, *J. Geophys. Res.* **93**, 9584.
Gary, S. P., Akimoto, K., and Winske, D.: 1989, *J. Geophys. Res.* **94**, 3513.
Gendrin, R., Ashour-Abdalla, M., Omura, Y., and Quest, K.: 1984, *J. Geophys. Res.* **89**, 9119.
Glassmeier, K. H., Coates, A. J., Acũna, M. H., Goldstein, M. L., Johnstone, A. D., Neubauer, F. M., and Rème, H.: 1989, *J. Geophys. Res.* **94**, 37.
Goldstein, M. L. and Wong, H. K.: 1987, *J. Geophys. Res.* **92**, 4695.
Goldstein, M. L., Smith, C. W., and Matthaeus, W. H.: 1983, *J. Geophys. Res.* **88**, 9989.
Goldstein, M. L., Wong, H. K., Viñas, A. F., and Smith, C. W.: 1985, *J. Geophys. Res.* **90**, 302.
Goldstein, M. L., Wong, H. K., and Eviatar, A.: 1986, *J. Geophys. Res.* **91**, 7954.
Gombosi, T. I.: 1988, *J. Geophys. Res.* **93**, 35.
Goodrich, C. C. and Lazarus, A. J.: 1976, *J. Geophys. Res.* **81**, 2750.
Gosling, J. T.: 1953, *Space Sci. Rev.* **34**, 113.
Gosling, J. T., Asbridge, J. R., Bame, S. J., Paschmann, G., and Sckopke, N.: 1978, *Geophys. Res. Letters* **5**, 957.
Gosling, J. T., Asbridge, J. R., Bame, S. J., Thomsen, M. F., and Zwickl, R. D.: 1986, *Geophys. Res. Letters* **13**, 267.
Gosling, J. T., Bame, S. J., Feldman, W. C., Paschmann, G., Sckopke, N., and Russell, C. T.: 1984, *J. Geophys. Res.* **89**, 5409.
Gosling, J. T., Thomsen, M. F., Bame, S. J., Feldman, W. C., Paschmann, G., and Sckopke, N.: 1982, *Geophys. Res. Letters* **9**, 1333.
Gosling, J. T., Thomsen, M. F., Bame, S. J., and Russell, C. T.: 1989a, *J. Geophys. Res.* **94**, 3555.
Gosling, J. T., Thomsen, M. F., Bame, S. J., and Russell, C. T.: 1989b, *J. Geophys. Res.* **94**, 10027.
Gribov, B. E., Kecskemety, K., Sagdeev, R. Z., Shapiro, V. D., Shevchenko, V. I., Somogyi, A. J., Szego, K., Erdos, G., Eroshenko, E. G., Gringauz, K. I., Keppler, E., Marsden, R. G., Remizov, A. P., Richter, A. K., Riedler, W., Schwingenschuh, K., and Wenzel, K.-P.: 1987, *Astron. Astrophys.* **187**, 293.
Hada, T., Kennel, C. F., and Terasawa, T.: 1987, *J. Geophys. Res.* **92**, 4423.
Hoppe, M. M. and Russell, C. T.: 1982, *Nature* **295**, 41.
Hoppe, M. M. and Russell, C. T.: 1983, *J. Geophys. Res.* **88**, 2021.
Hoppe, M. M., Russell, C. T., Frank, L. A., Eastman, T. E., and Greenstadt, E. W.: 1981, *J. Geophys. Res.* **86**, 4471.
Hoshino, M. and Terasawa, T.: 1985, *J. Geophys. Res.* **90**, 57.
Ip, W.-H. and Axford, W. I.: 1986, *Planetary Space Sci.* **34**, 1061.
Isenberg, P. A.: 1987, *J. Geophys. Res.* **92**, 8795.
Johnstone, A. D., Coates, A. J., Heath, J., Thomsen, M. F., Wilken, B., Jockers, K., Formisano, V., Amata, E., Winningham, J. D., Borg, H., and Bryant, D. A.: 1987, *Astron. Astrophys.* **187**, 25.
Kan, J. R. and Swift, D. W.: 1983, *J. Geophys. Res.* **88**, 6919.
Kennel, C. F. and Engelmann, F.: 1966, *Phys. Fluids* **9**, 2377.
Kennel, C. F., Coroniti, F. V., Scarf, F. L., Livesey, W. A., Russell, C. T., Smith, E. J., Wenzel, K. P., and Scholer, M.: 1986, *J. Geophys. Res.* **91**, 11917.
Lakhina, G. S. and Buti, B.: 1976, *J. Geophys. Res.* **81**, 2135.
Le, G., Russell, C. T., and Smith, E. J.: 1989a, *J. Geophys. Res.* **94**, 3755.
Le, G., Russell, C. T., Gary, S. P., Smith, E. J., Riedler, W., and Schwingenschuh, K.: 1989b, *J. Geophys. Res.* **94**, 11989.
Lee, M. A.: 1982, *J. Geophys. Res.* **87**, 5063.
Lee, M. A.: 1983, *J. Geophys. Res.* **88**, 6109.
Lee, M. A. and Ip, W.-H.: 1987, *J. Geophys. Res.* **92**, 11041.
Lee, M. A. and Skadron, G.: 1985, *J. Geophys. Res.* **90**, 39.
Leubner, M. P. and Vinãs, A. F.: 1986, *J. Geophys. Res.* **91**, 13366.
Livi, S. and Marsch, E.: 1987, *J. Geophys. Res.* **92**, 7255.
Marsch, E. and Livi, S.: 1987, *J. Geophys. Res.* **92**, 7263.

Marsch, E., Muhlhauser, K.-H., Schwenn, R., Rosenbauer, H., Pilipp, W., and Neubauer, F. M.: 1982, *J. Geophys. Res.* **87**, 52.
Matthaeus, W. H. and Goldstein, M. L.: 1982, *J. Geophys. Res.* **87**, 6011.
Montgomery, M. D., Gary, S. P., Forslund, D. W., and Feldman, W. C.: 1975, *Phys. Rev. Letters* **35**, 667.
Montgomery, M. D., Gary, S. P., Feldman, W. C., and Forslund, D. W.: 1976, *J. Geophys. Res.* **81**, 2743.
Mukai, T., Miyake, W., Terasawa, T., Kitayama, M., and Hirao, K.: 1986, *Geophys. Res. Letters* **13**, 829.
Neubauer, F. M., Glassmeier, K. H., Pohl, M., Raeder, J., Acuna, M. H., Burlaga, L. F., Ness, N. F., Musmann, G., Mariani, F., Wallis, M. K., Ungstrup, E., and Schmidt, H. U.: 1986, *Nature* **321**, 352.
Neugebauer, M.: 1975, *J. Geophys. Res.* **80**, 998.
Neugebauer, M. and Neubauer, F. M.: 1988, *EOS, Trans. Am. Geophys. Union* **69**, 396.
Neugebauer, M., Lazarus, A. J., Altwegg, K., Balsiger, H., Goldstein, B. E., Goldstein, R., Neubauer, F. M., Rosenbauer, H., Schwenn, R., Shelley, E. G., and Ungstrup, E.: 1987a, *Astron. Astrophys.* **187**, 21.
Neugebauer, M., Neubauer, F. M., Balsiger, H., Fuselier, S. A., Goldstein, B. E., Goldstein, R., Mariani, F., Rosenbauer, H., Schwenn, R., and Shelley, E. G.: 1987b, *Geophys. Res. Letters* **14**, 995.
Neugebauer, M., Lazarus, A. J., Balsiger, H., Fuselier, S. A., Neubauer, F. M., and Rosenbauer, H.: 1989, *J. Geophys. Res.* **94**, 5227.
Omidi, N. and Winske, D.: 1986, *Geophys. Res. Letters* **13**, 397.
Omidi, N. and Winske, D.: 1987, *J. Geophys. Res.* **92**, 13409.
Omidi, N. and Winske, D.: 1988, *Geophys. Res. Letters* **15**, 1303.
Omidi, N. and Winske, D.: 1990, *J. Geophys. Res.* **95**, 2281.
Paschmann, G., Sckopke, N., Papamastorakis, I., Asbridge, J. R., Bame, S. J., and Gosling, J. T.: 1981, *J. Geophys. Res.* **86**, 4355.
Paschmann, G., Sckopke, N., Bame, S. J., and Gosling, J. T.: 1982, *Geophys. Res. Letters* **9**, 881.
Paschmann, G., Haerendel, G., Sckopke, N., Mobius, E., Luhr, H., and Carlson, C. W.: 1988, *J. Geophys. Res.* **93**, 11279.
Price, C. P. and Wu, C. S.: 1987, *Geophys. Res. Letters* **14**, 856.
Quest, K. B., Forslund, D. W., Brackbill, J. U., and Lee, K.: 1983, *Geophys. Res. Letters* **10**, 471.
Quest, K. B.: 1988, *J. Geophys. Res.* **93**, 9649.
Riedler, W., Schwingenschuh, K., Yeroshenko, Ye. G., and Styashkin, V. A.: 1986, *Nature* **321**, 288.
Rogers, B., Gary, S. P., and Winske, D.: 1985, *J. Geophys. Res.* **90**, 9494.
Russell, C. T.: 1972, *Planetary Space Sci.* **20**, 1541.
Sagdeev, R. Z., Shapiro, V. D., Shevchenko, V. I., and Szego, K.: 1986, *Geophys. Res. Letters* **13**, 85.
Saito, T., Yumoto, K., Hirao, K., Nakagawa, T., and Saito, K.: 1986, *Nature* **321**, 303.
Sanderson, T. R., Reinhard, R., van Nes, P., Wenzel, K. P., Smith, E. J., and Tsurutani, B. T.: 1985, *J. Geophys. Res.* **90**, 3973.
Schwartz, S. J., Kessel, R. L., Brown, C. C., Woolliscroft, L. J. C., Dunlop, M. W., Farrugia, C. J., and Hall, D. S.: 1988, *J. Geophys. Res.* **93**, 11295.
Sckopke, N., Paschmann, G., Bame, S. J., Gosling, J. T., and Russell, C. T.: 1983, *J. Geophys. Res.* **88**, 6121.
Sentman, D. D., Edmiston, J. P., and Frank, L. A.: 1981, *J. Geophys. Res.* **86**, 7487.
Skadron, G., Holdaway, R. D., and Lee, M. A.: 1988, *J. Geophys. Res.* **93**, 11354.
Smith, C. W. and Gary, S. P.: 1987, *J. Geophys. Res.* **92**, 117.
Smith, C. W. and Lee, M. A.: 1986, *J. Geophys. Res.* **91**, 81.
Smith, C. W., Goldstein, M. L., and Matthaeus, W. H.: 1983, *J. Geophys. Res.* **88**, 5581; Correction, 1984, *ibid.* **89**, 9159.
Smith, C. W., Goldstein, M. L., Gary, S. P., and Russell, C. T.: 1985, *J. Geophys. Res.* **90**, 1429.
Smith, E. J., Tsurutani, B. T., Chenette, D. L., Conlon, T. F., and Simpson, J. A.: 1976, *J. Geophys. Res.* **81**, 65.
Smith, E. J., Tsurutani, B. T., Slavin, J. A., Jones, D. E., Siscoe, G. L., and Mendis, D. A.: 1986, *Science* **232**, 382.
Stix, T. H.: 1962, *The Theory of Plasma Waves*, McGraw-Hill Book Co., New York.
Takahashi, K. and Hones, E. W., Jr.: 1988, *J. Geophys. Res.* **93**, 8558.
Thomas, V. A. and Brecht, S. H.: 1986, *Phys. Fluids* **29**, 3398.
Thomas, V. A. and Brecht, S. H.: 1988, *J. Geophys. Res.* **93**, 11341.
Thomsen, M. F.: 1985, 'Upstream Suprathermal Ions', in *Collisionless Shocks in the Heliosphere: Reviews of Current Research*, American Geophysical Union, Washington, D.C., p. 253.
Thomsen, M. F., Gosling, J. T., Bame, S. J., and Russell, C. T.: 1985, *J. Geophys. Res.* **90**, 267.

Thomsen, M. F., Gosling, J. T., Bame, S. J., Quest, K. B., Russell, C. T., and Fuselier, S. A.: 1988, *J. Geophys. Res.* **93**, 11311.
Thorne, R. M. and Tsurutani, B. T.: 1987, *Planetary Space Sci.* **35**, 1501.
Tsurutani, B. T. and Smith, E. J.: 1984, *Geophys. Res. Letters* **11**, 331.
Tsurutani, B. T. and Smith, E. J.: 1986a, *Geophys. Res. Letters* **13**, 259.
Tsurutani, B. T. and Smith, E. J.: 1986b, *Geophys. Res. Letters* **13**, 263.
Tsurutani, B. T., Smith, E. J., and Jones, D. E.: 1983, *J. Geophys. Res.* **88**, 5645.
Tsurutani, B. T., Richardson, I. G., Thorne, R. M., Butler, W., Smith, E. J., Cowley, S. W. H., Gary, S. P., Akasofu, S.-I., and Zwickl, R. D.: 1985, *J. Geophys. Res.* **90**, 12159; Correction, 1986, *ibid.* **91**, 4606.
Tsurutani, B. T., Thorne, R. M., Smith, E. J., Gosling, J. T., and Matsumoto, H.: 1987a, *J. Geophys. Res.* **92**, 11074.
Tsurutani, B. T., Brinca, A. L., Smith, E. J., Thorne, R. M., Scarf, F. L., Gosling, J. T., and Ipavich, F. M.: 1987b, *Astron. Astrophys.* **187**, 97.
Tsurutani, B. T., Page, D. E., Smith, E. J., Goldstein, B. E., Brinca, A. L., Thorne, R. M., Matsumoto, H., Richardson, I. G., and Sanderson, T. R.: 1989a, *J. Geophys. Res.* **94**, 18.
Tsurutani, B. T., Brinca, A. L., Buti, B., Smith, E. J., Thorne, R. M., and Matsumoto, H.: 1989b, *J. Geophys. Res.* **94**, 29.
Unti, T. and Russell, C. T.: 1976, *J. Geophys. Res.* **81**, 469.
Verigin, M. I., Gringauz, K. I., Richter, A. K., Gombosi, T. I., Remizov, A. P., Szego, K., Apathy, I., Szemerey, I., Tatrallyay, M., and Lezhen, L. A.: 1987, *Astron. Astrophys.* **187**, 121.
Viñas, A. F., Goldstein, M. L., and Acuña, M. H.: 1984, *J. Geophys. Res.* **89**, 3762.
Watanabe, Y. and Terasawa, T.: 1984, *J. Geophys. Res.* **89**, 6623.
Wilken, B., Johnstone, A., Coates, A., Borg, H., Amata, E., Formisano, V., Jockers, K., Rosenbauer, H., Studemann, W., Thomsen, M. F., and Winningham, J. D.: 1987, *Astron. Astrophys.* **187**, 153.
Winske, D. and Gary, S. P.: 1986, *J. Geophys. Res.* **91**, 6825.
Winske, D. and Leroy, M. M.: 1984, *J. Geophys. Res.* **89**, 2673.
Winske, D. and Leroy, M. M.: 1985, in H. Matsumoto and T. Sato (eds.), *Computer Simulations of Space Plasmas – Selected Lectures at the First ISSS*, Terra Publishers, D. Reidel Publ. Co., Dordrecht, Holland, p. 568.
Winske, D. and Quest, K. B.: 1986, *J. Geophys. Res.* **91**, 8789.
Winske, D., Wu, C. S., Li, Y. Y., and Guo, S. Y.: 1984, *J. Geophys. Res.* **89**, 7327.
Winske, D., Wu, C. S., Li, Y. Y., Mou, Z. Z., and Guo, S. Y.: 1985a, *J. Geophys. Res.* **90**, 2713.
Winske, D., Stover, E. K., and Gary, S. P.: 1985b, *Geophys. Res. Letters* **12**, 295.
Wu, C. S. and Davidson, R. C.: 1972, *J. Geophys. Res.* **77**, 5399.
Wu, C. S. and Hartle, R. E.: 1974, *J. Geophys. Res.* **79**, 283.
Wu, C. S., Winske, D., and Gaffey, J. D.: 1986, *Geophys. Res. Letters* **13**, 865.
Yumoto, K., Saito, T., and Nakagawa, T.: 1986, *Geophys. Res. Letters* **13**, 825.
Zachary, A. L., Cohen, B. I., Max, C. E., and Arons, J.: 1989, *J. Geophys. Res.* **94**, 2443.